

# Spectral properties of the 2D Holstein polaron

H. Fehske<sup>1</sup>, J. Loos<sup>2</sup> and G. Wellein<sup>1</sup>

<sup>1</sup>*Physikalisches Institut, Universität Bayreuth, D-95440 Bayreuth, Germany*

<sup>2</sup>*Institute of Physics, Czech Academy of Sciences, 16200 Prague, Czech Republic*  
(Bayreuth, 30 June 1997)

The two-dimensional Holstein model is studied by means of direct Lanczos diagonalization preserving the full dynamics and quantum nature of phonons. We present numerical exact results for the single-particle spectral function, the polaronic quasiparticle weight, and the optical conductivity. The polaron band dispersion is derived both from exact diagonalization of small lattices and analytic calculation of the polaron self-energy.

## I. INTRODUCTION

Research on polarons has recently gained renewed interest on account of the observation of polaronic effects in several important classes of materials with perovskite related structure, such as the bismuthates ( $\text{Ba}_{1-x}\text{K}_x\text{BiO}_3$ ), the high- $T_c$  cuprates (e.g.,  $\text{La}_{2-x}\text{Sr}_x\text{CuO}_4$ ), the non-metallic nickelates ( $\text{La}_{2-x}\text{Sr}_x\text{NiO}_4$ ), or the colossal magnetoresistive manganites (e.g.,  $\text{La}_{1-x}\text{Ca}_x\text{MnO}_3$ ) [1]. Despite a more than a half-century of theoretical and experimental study, our understanding of the formation and transport properties of polarons and bipolarons is still incomplete. Even the very fundamental problem of a single tight-binding electron coupled locally to a set of non-interacting Einstein oscillators (Holstein model [2]) has not been solved exactly, i.e., no satisfactory description of the full spectral properties has been obtained so far. That is because the standard analytical techniques, based, e.g., on variational approaches [3] or on weak-coupling [4] and strong-coupling adiabatic [2] and non-adiabatic [5,6] perturbation expansions, fail to tackle this complicated many-body problem precisely in the physically most important transition region, where the highly non-linear “self-trapping” process from an essentially delocalized quasi-free charge carrier at weak electron-phonon (EP) interaction to a “quasi-localized” small polaron at strong coupling takes place. Note that the same problem arises in strongly coupled exciton-phonon systems as well [7].

As an attempt to close the gap between the weak and strong EP coupling limits, in this paper we investigate the Holstein model on finite lattices mainly employing approximation-free diagonalization techniques which, at the moment, provide the only reliable tool for studying polarons close to the crossover regime.

Explicitly we write the Holstein Hamiltonian

$$\mathcal{H} = -t \sum_{\langle ij \rangle} (c_i^\dagger c_j + c_j^\dagger c_i) + \omega_b \sum_i (b_i^\dagger b_i + \frac{1}{2})$$

$$- \sqrt{\varepsilon_p \omega_b} \sum_i (b_i^\dagger + b_i) c_i^\dagger c_i, \quad (1)$$

where  $c_i^{[\dagger]}$  and  $b_i^{[\dagger]}$  are the annihilation [creation] operators of a (spinless) fermion and a boson (phonon) at Wannier site  $i$ , respectively. In (1), the free electron transfer ( $t$ ) is restricted to nearest-neighbour (NN) pairs ( $\langle ij \rangle$ ), the phonons are treated within harmonic approximation, and the EP term introduces a coupling between the local electron density and the dispersionsless optical phonon mode. Denoting by  $g$  the dimensionless EP interaction constant,  $\varepsilon_p = g^2 \omega_b$  is the Lang-Firsov strong-coupling polaron binding energy with  $\omega_b$  as the bare phonon frequency.

The single-electron Holstein model has been studied extensively as a paradigmatic model for polaron formation in systems with dominant short-range electron-lattice interactions. The principal result is that irrespective of the adiabaticity ratio,  $\alpha = \omega_b/t$ , small polarons will be formed in a  $D$ -dimensional system provided that the *two* conditions  $\lambda = \varepsilon_p/2Dt > 1$  and  $g^2 > 1$  are fulfilled (see Fig. 1). In the weak-coupling (adiabatic) limit, one expects (from scaling arguments) a quasi-free electron behaviour for  $D > 1$ , while in a 1D system the carrier state becomes polaronic at arbitrary small  $\lambda$  (“large” polaron). Previous exact diagonalization (ED) work has concentrated on the 1D case [8–12,21,13–17], where, however, the calculations were limited to either very small clusters, rather weak EP coupling ( $\lambda < 1$ ) or to the adiabatic limit ( $\omega_b = 0$ ). On the other hand, the most interesting effects will be expected if the characteristic electronic and phononic energy scales are not well separated ( $\lambda \sim 1$ ;  $\alpha \sim 1$ ). For example, very recent numerical investigations, performed in the crossover region for 1D chains with up to 20 sites, indicate that the polaronic band structure markedly deviates from a simple tight-binding dispersion [18–20].

Our purpose here is to extend these studies to 2D systems and explore the spectral properties of the 2D Holstein model, whereby the focus is on the *intermediate* EP coupling and phonon frequency regime. Section 2 presents the ED results for the single-particle spectral function and the optical conductivity. In Sect. 3 we outline an analytical approach based on an “incomplete” Lang-Firsov transformation, to calculate second-order corrections to the polaronic self-energy. Section 4 contains a discussion of the polaronic band dispersion, where the ED data are used to test the validity of the proposed theory. The principal results are summarized in Sec. 5.

## II. NUMERICAL APPROACH

Performing direct diagonalizations of the Holstein model on finite ( $N$ -site) square lattices with periodic boundary conditions (PBC), we exploit the translational invariance by the use of symmetrized basis sets in the tensorial product Hilbert space of electronic and phononic states

$$\{|\vec{K}; s\rangle\} = \sum_{i=1}^N \frac{e^{i\vec{K}\vec{R}_i}}{\sqrt{N}} \mathcal{T}_{\vec{R}_i} (|1, 0, \dots, 0\rangle_{el} \otimes \{|s\rangle_{ph}\}). \quad (2)$$

Here  $\mathcal{T}_{\vec{R}_i}$  describes the allowed lattice translations and  $\vec{K}$  is the *total* momentum of the coupled EP system. Since the Hilbert space associated with the phonons is infinite even for a finite system, we apply a truncation procedure [22,13] restricting ourselves to phononic states  $|s\rangle_{ph} = \prod_{i=1}^N \frac{1}{\sqrt{n_i^s!}} (b_i^\dagger)^{n_i^s} |0\rangle_{ph}$  with at most  $M$  phonons. That means, we take into account all  $m$ -phonon states, where  $m = \sum_{i=1}^N n_i^s \leq M$ ,  $n_i^s \in [0, m]$  and  $1 \leq s \leq D_{ph}^{(M)}$ . Here  $D_{ph}^{(M)} = (M+N)!/M!N!$  denotes the dimension of the phononic Hilbert space. Then a  $\vec{K}$ -symmetrized state of the Holstein model is given as

$$|\Psi_{\vec{K}}\rangle = \sum_{m=0}^M \sum_{\bar{s}=1}^{\bar{S}(m)} c_{\vec{K}}^{m,\bar{s}} |\vec{K}; m, \bar{s}\rangle, \quad (3)$$

where  $\bar{S}(m) = (N-1+m)!/(N-1)!m!$ .

Needless to say, that we have carefully to check for the convergence of both the ground-state energy,  $E_0(M)$ , and the phonon distribution,  $|c^m|^2(M) = \sum_{\bar{s}} |c_{\vec{K}=0}^{m,\bar{s}}|^2$ , as a function of the maximal number of phonons retained [13]. Implementing an improved Lanczos algorithm on parallel computers, we are able to calculate the ground-state properties of systems with a total dimension of about  $10^7$ . To obtain information about dynamical properties, we combine the Lanczos diagonalization with the Chebyshev recursion and maximum entropy methods, which are very efficient for high-energy resolution applications [23].

### A. Single-particle spectral function

By examining the dynamical properties of polarons, of particular importance is whether a quasiparticle-like excitation exists in the spectrum. In order to discuss this issue we have evaluated the wave-vector resolved spectral density function

$$\mathcal{A}_{\vec{K}}(E) = \sum_n |\langle \Psi_{n,\vec{K}} | c_{\vec{K}}^\dagger | 0 \rangle|^2 \delta(E - E_{n,\vec{K}}), \quad (4)$$

where  $c_{\vec{K}}^\dagger$  creates an electron with momentum  $\vec{K}$ ;  $|0\rangle$  is the vacuum state (containing no phonons). For a finite system, the eigenvalues  $E_{n,\vec{K}}$  and eigenstates  $|\Psi_{n,\vec{K}}\rangle$  in

the single-particle subspace can be obtained from ED. As stated above, we prefer to use a moment expansion method in order to calculate  $\mathcal{A}_{\vec{K}}(E)$  directly.

In Fig. 2,  $\mathcal{A}_{\vec{K}}(E)$  is displayed for two different EP couplings  $\lambda = 0.125$  (a-c) and  $\lambda = 1.25$  (d-f) (corresponding to the weak and intermediate-to-strong coupling situations, respectively) at the allowed  $\vec{K}$ -vectors of the 18-site square lattice. To visualize the intensities (spectral weights) connected with the various peaks (excitations) we also have shown the integrated density of states

$$\mathcal{N}_{\vec{K}}(E) = \int_{-\infty}^E dE' \mathcal{A}_{\vec{K}}(E'). \quad (5)$$

Let us first consider the weak-coupling case. Owing to the ‘‘hybridization’’ of electron and phonon degrees of freedom, we found in each  $\vec{K}$ -sector excitations being separated from the ground state by an energy of about  $\omega_b$ . As can be seen from  $\mathcal{N}_{\vec{K}}(E)$ , however, these predominantly phononic states have only a small admixture of electronic character, i.e., the main spectral weight is still located at energies that correspond to the bare tight-binding levels  $\epsilon_{\vec{K}} = -2t(\cos K_x + \cos K_y)$ . Other (satellite) peaks appear due to the existence of higher excited multi-phonon states. Increasing the EP interaction, we notice significant changes in the spectral function as  $\varepsilon_p$  exceeds half the bare bandwidth. Most notably, a band of polaronic states with low spectral weight evolves. This so-called small polaron band becomes extremely narrow and is well-separated from the rest of the spectra in the strong-coupling limit ( $\lambda \gg 1$ ). At the same time spectral weight is redistributed to the high-energy part of the spectra.

To elucidate the nature of the ground state in more detail, in Fig. 3 a we have plotted the phonon distribution in the ground state at several EP interaction strengths and phonon frequencies. The results unambiguously confirm the importance of multi-phonon states especially in the strong-coupling regime ( $g^2 \gg 1$ ), where  $|c^m|^2$  becomes the usual Poisson distribution for small polarons. Here the phonons will heavily dress the electron and as a result the bare electron no longer behaves like a well-defined quasiparticle. In fact, this is exactly what has been observed in Fig. 2 d, where the residue of the quasiparticle peak at  $\vec{K} = 0$ ,

$$\mathcal{Z}^{(c)} = |\langle \Psi_{0,\vec{K}} | c_{\vec{K}}^\dagger | 0 \rangle|_{\vec{K}=0}^2, \quad (6)$$

is weakened. Then the question arises whether one can construct an appropriate quasiparticle operator having large spectral weight at the lowest pole in the spectrum. This point was intensively discussed in the context of strongly correlated electron models (e.g., for the t-J model) for the case of an additional hole injected in the antiferromagnetic ground state of the undoped system [24] and, more recently, similar ideas have been addressed for strongly coupled EP systems as well [16,25]. Of course, in the parameter regime  $\lambda \gg 1$ ,  $\alpha > 1$  the

small polaron defined through the Lang–Firsov transformation [5] (cf. Sec. 3) is a good quasiparticle. This was explicitly demonstrated in recent ED work [16].

To tackle the intermediate coupling and frequency regime, we construct a composite polaron operator with momentum  $\vec{K}$  on the basis of the phonon distribution function,

$$d_{\vec{K}}^\dagger = \sqrt{\frac{1}{N}} \sum_{i=1}^N e^{i\vec{K}\cdot\vec{R}_i} c_i^\dagger \sum_{m=0}^M \sqrt{\frac{|c^m(M)|^2}{m!}} (b_i^\dagger)^m, \quad (7)$$

keeping in mind that the polaronic state is characterized by strong on-site EP correlations. In Fig. 3 b, we have compared the quasiparticle weight factor  $Z^{(d)}$ , computed by the use of the dressed electron operator (7), with the spectral weight simply given by (6). As expected, the results for  $Z^{(d)}$  are actually very close to those for  $Z^{(c)}$  at weak enough EP coupling. Clearly, in this case the phonon distribution is sharply peaked at the zero-phonon state (cf. Fig. 3 a) and the particle behaves as a nearly free electron. By contrast, if one increases the EP coupling strength, both electrons and phonons lose their own identity by forming polarons. Concomitantly we observe less “electronic character” of the polaronic quasiparticle and, indeed, it can be shown analytically that (in the bulk limit)  $Z^{(c)}$  vanishes exponentially at very large couplings ( $\lambda \gg 1$ ). On the other hand, although care must be taken in the interpretation of our finite-cluster data for  $Z$ , the large value found for  $Z^{(d)}$  suggests that the proposed  $d$ -operator correctly describes the phonon dressing of the quasiparticle even in the transition regime. Accordingly the position of the maxima in the distribution function provides an estimate of the (most probable) number of phonons contained in the “phonon-cloud” of the small polaron.

## B. Optical conductivity

In linear response theory the real part of the optical conductivity is given by [24]

$$\text{Re}\sigma_{xx}(\omega) = \mathcal{D}\delta(\omega) + \sigma_{xx}^{reg}(\omega), \quad (8)$$

where  $\mathcal{D}$  denotes the Drude weight and the second term (sometimes called incoherent or regular part of the conductivity) can be written in a spectral representation as

$$\sigma_{xx}^{reg} = \frac{e^2\pi}{N} \sum_{m \neq 0} \frac{|\langle \Psi_0 | \hat{j}_x^{(p)} | \Psi_m \rangle|^2}{E_m - E_0} \delta(\omega - E_m + E_0). \quad (9)$$

For the Holstein model the (paramagnetic) current density operator has the form

$$\hat{j}_x^{(p)} = it \sum_i (c_i^\dagger c_{i+x} - c_{i+x}^\dagger c_i). \quad (10)$$

According to the  $f$ -sum rule the integrated conductivity is related to the ground-state expectation value of the kinetic energy operator

$$\mathcal{H}_t = -t \sum_{\langle ij \rangle} (c_i^\dagger c_j + c_j^\dagger c_i). \quad (11)$$

By introducing the  $\omega$ -integrated weight  $\mathcal{S}^{reg} = \mathcal{S}^{reg}(\infty)$ ,

$$\mathcal{S}^{reg}(\omega) = \int_0^\omega d\omega' \sigma_{xx}^{reg}(\omega'), \quad (12)$$

and integrating in  $\omega$  both terms on the r.h.s. of (8), one arrives at

$$\mathcal{S}^{tot} = \frac{\pi e^2}{4} \langle -\mathcal{H}_t \rangle = \frac{\mathcal{D}}{2} + \mathcal{S}^{reg}. \quad (13)$$

As pointed out by Emin [26], there are two simple limits in which absorption associated with photoionization of Holstein polarons is well understood and the optical conductivity can be calculated analytically. The first one is the weak-coupling case, where the absorption coefficient falls monotonically with increasing applied frequency. In the opposite strong-coupling (small polaron) limit, the optical properties are dominated by (incoherent) small polaron hopping processes accompanied by multi-phonon absorptions and emissions (i.e., by non-diagonal transitions [27]). As a result the absorption is peaked about  $\omega \sim 2\varepsilon_p$ , whereby, in contrast to the case of large (Fröhlich-type) polarons, the low-frequency side is evaluated above the high-frequency side of the absorption peak [26]. Recently, for the weak-, intermediate- and strong-coupling regimes absorption spectra are obtained with numerical calculation of the finite-frequency part of the optical conductivity of (1D) finite-size Holstein models with up to four-sites [28,15].

Since it is not expected that the dimensionality (cluster size) plays a crucial role in the extreme small polaron limit, in the discussion of the optical response we again focus on the crossover region. Results are presented in Fig. 4. The upper panel shows the frequency dependence of the optical conductivity (omitting the Drude contribution, i.e., the intra-band transitions). The most interesting qualitative feature of the absorption spectrum seems to be the strongly asymmetric lineshape. The low-frequency peak structure may be easily understood in connection with the single-particle spectra. For example, an inspection of Fig. 2 d–f verifies that the first/second group of peaks correspond to inter-band transitions from the  $\vec{K} = (0,0)$  ground state to states with finite momenta, triggered by one/two phonon absorption processes ( $\omega \sim E_{0,\vec{K}} - E_0 + n\omega_b$ , where  $\omega_b = 1.5$  and  $(E_{0,\vec{K}} - E_0) \sim 0.5$  for  $\vec{K}=(1,1), (2,0), (2,2), (3,1), (3,3)$  [see also Fig. 5 a below]). In principle such processes are possible even at arbitrarily small EP coupling because there is always a finite overlap of the corresponding wave-functions. However, the peak strength rapidly

decreases if the EP coupling becomes weaker. This can be seen from the inset of Fig. 4 a, by comparing the integrated weight  $\mathcal{S}^{reg}(\omega)$  in the dissipative part of  $\sigma(\omega)$ .

To analyze the role of the EP coupling strength on the optical response in more detail, we have displayed  $\mathcal{S}^{reg}$  together with the total sum rule (kinetic energy) in Fig. 4 b.  $\mathcal{S}^{tot}$  is directly related to the effective polaronic hopping amplitude,  $t_{p,eff} = \mathcal{S}^{tot}/\pi e^2$ , which can be taken as a measure of a polaron's mobility [13,21]. Containing both coherent and incoherent transport processes,  $t_{p,eff}$  substantially differs from the (exponential) polaron band renormalization factors obtained analytically in the adiabatic Holstein and non-adiabatic Lang-Firsov cases [12] (cf. Appendix). Fig. 4 b clearly shows the crossover from a nearly free electron, characterized by a  $t_{p,eff}$  that is only weakly reduced from its non-interacting value ( $t_{p,eff}(\lambda = 0) = 1$ ), to a less mobile small (Holstein/Lang-Firsov) polaron in the (adiabatic/non-adiabatic) strong-coupling limit. Concomitantly, in the weak-coupling regimes nearly all the spectral weight stays in the Drude part. As previously found for the (1D) four-site Holstein cluster [15], the sharp decrease of  $\mathcal{S}^{tot}$  in the crossover region is driven by the fall of the Drude weight. By contrast the optical absorption due to inelastic scattering processes, described by the regular part of the optical conductivity, becomes enhanced in the transition region. Of course,  $\mathcal{S}^{reg}$  also decreases as  $\lambda$  increases in the extreme strong-coupling regime.

### III. THEORETICAL APPROACH

In this section we treat the intermediate-to-strong EP coupling regime analytically, applying the Green's function formalism advocated by Schnakenberg [29] to the polaron problem. We start with the Holstein Hamiltonian (1) transformed by the *incomplete* Lang-Firsov transformation  $\mathcal{U} = \exp\{\gamma g \sum_i (b_i^\dagger - b_i) c_i^\dagger c_i\}$ ,  $\tilde{\mathcal{H}} = \mathcal{U}^\dagger \mathcal{H} \mathcal{U}$  [5,30]:

$$\tilde{\mathcal{H}} = \eta \sum_i c_i^\dagger c_i - \sum_{i,j} \mathcal{C}_{ij} c_i^\dagger c_j + \omega_b \sum_i (b_i^\dagger b_i + \frac{1}{2}), \quad (14)$$

where

$$\eta = -\varepsilon_p \gamma (2 - \gamma) - \mu, \quad (15)$$

$$\mathcal{C}_{ii} = g \omega_b (1 - \gamma) (b_i^\dagger + b_i), \quad (16)$$

$$\mathcal{C}_{ij} = t \Phi_{\langle ij \rangle} = t \exp\{-\gamma g (b_i^\dagger - b_i - b_j^\dagger + b_j)\}. \quad (17)$$

In (14), the (variational) parameter  $\gamma$  measures the degree of the dynamical polaron effect ( $0 \leq \gamma \leq 1$ );  $\mu$  is the chemical potential.

The Green's function equations of motion deduced from  $\tilde{\mathcal{H}}$  lead to a set of coupled equations for generalized polaron ( $c$ - $c$ ) and "mixed" ( $c$ - $\mathcal{C}$ ) Green's functions; the equation for the generalized polaron Green's function

may be converted into an equation for the generalized self-energy and solved by iteration (see Refs. [29,31,32] for details). In the second step of iteration, the polaron self energy is obtained as

$$\begin{aligned} \Sigma^{(2)}(\vec{m}_1 \tau_1; \vec{m}_2 \tau_2) = & -\langle \mathcal{C}_{\vec{m}_1 \vec{m}_2} \rangle \delta(\tau_1 - \tau_2) \quad (18) \\ & + \sum_{\vec{m}' \vec{m}''} \mathcal{G}(\vec{m}' \tau_1; \vec{m}'' \tau_2) [\langle \mathcal{T}_\tau \mathcal{C}_{\vec{m}_1 \vec{m}'}(\tau_1) \mathcal{C}_{\vec{m}'' \vec{m}_2}(\tau_2) \rangle \\ & - \langle \mathcal{C}_{\vec{m}_1 \vec{m}'} \rangle \langle \mathcal{C}_{\vec{m}'' \vec{m}_2} \rangle], \end{aligned}$$

where the  $\tau$ -dependence of the boson operators  $b_i^{[\dagger]}$  and the statistical averages are to be determined using the Hamiltonian of independent local oscillators (the last term on the r.h.s. of (14)). Introducing the abbreviations  $\mathcal{W}(\vec{m}_1 \vec{m}'; \vec{m}_2 \vec{m}''; \tau)$  for the expression in the square brackets of (18) [the  $\vec{m}_i$ ,  $\vec{m}'$ , and  $\vec{m}''$  refer to lattice vectors, and  $\tau = \tau_1 - \tau_2$ ], the Fourier transformation of (18) gives the self-energy equation in the space of Brillouin zone  $\vec{K}$ -vectors and Matsubara frequencies  $i\omega_\nu = i(2\nu + 1)\pi/\beta$ , i.e.,

$$\begin{aligned} \Sigma_{\vec{K}}^{(2)}(i\omega_\nu) = & - \sum_{\vec{m}_2 - \vec{m}_1} \langle \mathcal{C}_{\vec{m}_1 \vec{m}_2} \rangle e^{i\vec{K}(\vec{m}_2 - \vec{m}_1)} \quad (19) \\ & + \sum_{\vec{m}_2 - \vec{m}_1} e^{i\vec{K}(\vec{m}_2 - \vec{m}_1)} \frac{1}{N} \sum_{\vec{K}', \varsigma; \vec{m}' \vec{m}''} e^{i\vec{K}'(\vec{m}' - \vec{m}'')} \mathcal{G}_{\vec{K}'}(i\omega_\varsigma) \\ & \times \frac{1}{\beta} \int_0^\beta d\tau e^{i(\omega_\nu - \omega_\varsigma)\tau} \mathcal{W}(\vec{m}_1 \vec{m}'; \vec{m}_2 \vec{m}''; \tau). \end{aligned}$$

Owing to the properties of  $\mathcal{C}_{ij}$ , the first approximation to the self energy,  $\Sigma_{\vec{K}}^{(1)}$ , given by the first term on the r.h.s. of (19), is non-zero only for elementary translations  $\vec{h} = \vec{m}_2 - \vec{m}_1$  connecting the site  $\vec{m}_1$  with the NN sites  $\vec{m}_2$ ; consequently, the  $\vec{K}$ -dependence of this term is given by  $2(\cos K_x + \cos K_y)$ . The terms obtained in the second step of iteration yield, besides for the case  $\vec{m}_2 - \vec{m}_1 = 0$ , non-zero contributions only for  $\vec{h}' = \vec{m}_2 - \vec{m}_1$  (vector from  $\vec{m}_1$  to next NN site  $\vec{m}_2$ ) and  $\vec{m}_2 - \vec{m}_1 = 2\vec{h}$  leading to the  $\vec{K}$ -functions  $4 \cos K_x \cos K_y$  and  $2(\cos 2K_x + \cos 2K_y)$ , respectively. In fact, denoting the NN sites to  $\vec{m}_1$  and  $\vec{m}_2$  by  $\vec{m}_1 + \vec{d}_1$  and  $\vec{m}_2 + \vec{d}_2$ , respectively, the non-vanishing  $\mathcal{W}(\vec{m}_1 \vec{m}'; \vec{m}_2 \vec{m}''; \tau)$  are given by

$$\mathcal{W}(\vec{m}, \vec{m} + \vec{d}_1; \vec{m}, \vec{m} + \vec{d}_1; \tau) = t^2 \mathcal{F}_1(\tau; 2\tilde{g}^2) \quad (20)$$

for  $\vec{m}_1 = \vec{m}_2 = \vec{m}$  and  $\vec{d}_1 = \vec{d}_2$ ,

$$\mathcal{W}(\vec{m}, \vec{m} + \vec{d}_1; \vec{m}, \vec{m} + \vec{d}_2; \tau) = t^* t \mathcal{F}_1(\tau; \tilde{g}^2) \quad (21)$$

for  $\vec{m}_1 = \vec{m}_2 = \vec{m}$  and  $\vec{d}_1 \neq \vec{d}_2$ ,

$$\mathcal{W}(\vec{m}_1, \vec{m}_1 + \vec{d}_1; \vec{m}_2, \vec{m}_2 + \vec{d}_2; \tau) = t^* t \mathcal{F}_1(\tau; \tilde{g}^2) \quad (22)$$

for  $\vec{m}_2 - \vec{m}_1 = \vec{h}'$ ,  $2\vec{h}$  and simultaneously  $\vec{m}_1 + \vec{d}_1 = \vec{m}_2 + \vec{d}_2$ ,

$$\begin{aligned}\mathcal{W}(\vec{m}, \vec{m} + \vec{d}_1; \vec{m}, \vec{m}; \tau) &= \mathcal{W}(\vec{m}, \vec{m}; \vec{m}, \vec{m} + \vec{d}_2; \tau) \\ &= t^* \gamma (1 - \gamma) \varepsilon_p \mathcal{F}_2(\tau)\end{aligned}\quad (23)$$

for  $\vec{m}_2 - \vec{m}_1 = 0$ ,

$$\begin{aligned}\mathcal{W}(\vec{m}_1, \vec{m}_2; \vec{m}_2, \vec{m}_2; \tau) &= \mathcal{W}(\vec{m}_1, \vec{m}_1; \vec{m}_2, \vec{m}_1; \tau) \\ &= -t^* \gamma (1 - \gamma) \varepsilon_p \mathcal{F}_2(\tau)\end{aligned}\quad (24)$$

for  $\vec{m}_2 - \vec{m}_1 = \vec{h}$ , and

$$\mathcal{W}(\vec{m}, \vec{m}; \vec{m}, \vec{m}; \tau) = \varepsilon_p (1 - \gamma)^2 \omega_b \mathcal{F}_3(\tau). \quad (25)$$

Here,  $t^* = t \exp\{-\tilde{g}^2 \coth \vartheta\}$ ,  $\tilde{g} = \gamma g$  and the functions  $\mathcal{F}_{1,2,3}$  are defined as follows

$$\begin{aligned}F_1(\tau, \kappa) &= \exp\{-\kappa \coth \vartheta\} \\ &\times \left[ 2 \sum_{s=1}^{\infty} I_s(\zeta) \cosh[s(\vartheta - \omega_b \tau)] + I_0(\zeta) - 1 \right],\end{aligned}\quad (26)$$

$$F_2(\tau) = \sinh(\vartheta - \omega_b \tau) / \sinh \vartheta, \quad (27)$$

$$F_3(\tau) = \bar{n} \exp\{\omega_b \tau\} + (\bar{n} + 1) \exp\{-\omega_b \tau\}, \quad (28)$$

where  $\vartheta = \beta \omega_b / 2$ ,  $\bar{n} = [\exp\{\beta \omega_b\} - 1]^{-1}$ ,  $\zeta = \kappa / \sinh \vartheta$ , and  $I_s(\zeta)$  denote the modified Bessel functions.

Deriving the above expressions of  $\mathcal{W}$ , the averages  $\langle \dots \rangle$  were evaluated applying [33]

$$\left\langle e^{Xb} e^{-Yb^\dagger} \right\rangle = \exp \left\{ \frac{-XY}{1 - \exp\{-\beta \omega_b\}} \right\}. \quad (29)$$

In particular, the functions originating from the  $\mathcal{T}_\tau$ -ordered products of  $\mathcal{C}_{ii}$  and  $\Phi_{ij}$  were calculated as  $\varepsilon$ -derivatives of the generating functional  $\langle \mathcal{T}_\tau(\exp\{\varepsilon[b_i^\dagger(\tau_1) + b_i(\tau_1)]\} \Phi_{ij}(\tau_2)) \rangle$  (at  $\varepsilon = 0$ ). After inserting (20)–(25) into (19), the  $\tau$ -integration is easily accomplished. As a next step, the summation over the Matsubara frequencies  $i\omega_\zeta$  has to be carried out. For this aim, the Green's function in (19) will be expressed by means of the spectral function  $\mathcal{A}_{\vec{K}'}(\omega')$ , i.e.,

$$\mathcal{G}_{\vec{K}'}(i\omega_\zeta) = \int_{-\infty}^{\infty} \frac{d\omega'}{2\pi} \mathcal{A}_{\vec{K}'}(\omega') \frac{1}{i\omega_\zeta - \omega'}, \quad (30)$$

and  $\mathcal{A}_{\vec{K}'}(\omega') = 2\pi \delta(\omega' - \xi_{\vec{K}'})$  will be assumed, where  $\xi_{\vec{K}'} = \eta + \Sigma_{\vec{K}'}^{(1)}$  is given by the first approximation of the quasiparticle energy. Further approximations that will be made in the explicit calculations are based (i) on the assumption  $\vartheta \gg 1$  (low-temperature approximation) and (ii) on the limitation to negligible carrier concentration. In this way we obtain

$$\begin{aligned}\frac{1}{N} \sum_{\vec{K}', \varsigma} \mathcal{G}_{\vec{K}'}(i\omega_\zeta) \frac{1}{\beta} \int_0^\beta d\tau e^{i(\omega_\nu - \omega_\zeta)\tau} F_1(\tau, \kappa) \\ = \sum_{s=1}^{\infty} e^{-\kappa} \frac{\kappa^s}{s!} \frac{1}{N} \sum_{\vec{K}'} \left[ \frac{n_B(s\omega_b) + n_F(\xi_{\vec{K}'})}{i\omega_\nu - \xi_{\vec{K}'} + s\omega_b} \right. \\ \left. + \frac{n_B(s\omega_b) + 1 - n_F(\xi_{\vec{K}'})}{i\omega_\nu - \xi_{\vec{K}'} - s\omega_b} \right].\end{aligned}\quad (31)$$

In view of (i) and (ii), we can neglect both  $n_B(s\omega_b)$  and  $n_F(\xi_{\vec{K}'})$  in (31). The contributions to the self energy determined by the functions  $\mathcal{F}_2(\tau)$  and  $\mathcal{F}_3(\tau)$  are treated in a quite analogous manner. Collecting all non-zero contributions to the r.h.s of (19) and performing the analytical continuation  $i\omega_\zeta \rightarrow \bar{\omega} = \omega + i\delta$  ( $\delta \rightarrow 0^+$ ), the following low-temperature formula results:

$$\begin{aligned}\Sigma_{\vec{K}}^{(2)}(\bar{\omega}) &= -2t^* (\cos K_x + \cos K_y) \\ &+ z t^2 \sum_{s=1}^{\infty} e^{-2\tilde{g}^2} \frac{(2\tilde{g}^2)^s}{s!} \frac{1}{N} \sum_{\vec{K}'} \mathcal{G}_{\vec{K}'}^{(1)}(\bar{\omega} - s\omega_b) \\ &+ t^* t \sum_{s=1}^{\infty} e^{-\tilde{g}^2} \frac{\tilde{g}^{2s}}{s!} \frac{1}{N} \sum_{\vec{K}', \vec{d}_1 \neq \vec{d}_2} e^{i\vec{K}'(\vec{d}_1 - \vec{d}_2)} \mathcal{G}_{\vec{K}'}^{(1)}(\bar{\omega} - s\omega_b) \\ &+ 2t^* t [4 \cos K_x \cos K_y + \cos 2K_x + \cos 2K_y] \\ &\times \sum_{s=1}^{\infty} e^{-\tilde{g}^2} \frac{\tilde{g}^{2s}}{s!} \frac{1}{N} \sum_{\vec{K}'} \mathcal{G}_{\vec{K}'}^{(1)}(\bar{\omega} - s\omega_b) \\ &+ 2t^* \gamma (1 - \gamma) \varepsilon_p \frac{1}{N} \sum_{\vec{K}', \vec{h}} e^{i\vec{K}'\vec{h}} \mathcal{G}_{\vec{K}'}^{(1)}(\bar{\omega} - \omega_b) \\ &- 4t^* \gamma (1 - \gamma) \varepsilon_p (\cos K_x + \cos K_y) \frac{1}{N} \sum_{\vec{K}'} \mathcal{G}_{\vec{K}'}^{(1)}(\bar{\omega} - \omega_b) \\ &+ (1 - \gamma)^2 \varepsilon_p \omega_b \frac{1}{N} \sum_{\vec{K}'} \mathcal{G}_{\vec{K}'}^{(1)}(\bar{\omega} - \omega_b).\end{aligned}\quad (32)$$

$\mathcal{G}_{\vec{K}}^{(1)}(w) = [w - \xi_{\vec{K}}]^{-1}$  denotes the first-order (Hartree-Fock) Green's function for independent quasiparticles having band energies  $\xi_{\vec{K}}$ ;  $z$  is the NN coordination number.

The polaron self energy given by (32) will be used to determine the polaron band dispersion. Namely, the quasiparticle energy is obtained as a function of  $\vec{K}$  by solving

$$\omega = \eta + \text{Re} \Sigma_{\vec{K}}^{(2)}(\bar{\omega}). \quad (33)$$

In the strong-coupling case  $\gamma$  near 1 and an extreme polaron band narrowing are expected; the corresponding (crude) approximation consists in the omission of terms arising owing to the ‘‘residual’’ EP interaction given by  $\mathcal{C}_{ii}$  and the neglect of  $(\omega - \xi_{\vec{K}'})$  with respect to the energy scale of the Poisson distribution of the oscillator energy fluctuations  $s\omega_b$ . Then the polaron band dispersion is explicitly obtained from (32) as follows

$$\begin{aligned}E_{\vec{K}}(\gamma)/4t &= -\lambda \gamma (2 - \gamma) - \frac{1}{\alpha} \left\langle \frac{1}{s} \right\rangle_{\kappa=2\gamma^2 g^2} \\ &- \frac{e^{-\gamma^2 g^2}}{2} (\cos K_x + \cos K_y) - \frac{e^{-\gamma^2 g^2}}{2\alpha} \left\langle \frac{1}{s} \right\rangle_{\kappa=\gamma^2 g^2} \\ &\times [4 \cos K_x \cos K_y + \cos 2K_x + \cos 2K_y],\end{aligned}\quad (34)$$

where  $\langle 1/s \rangle_\kappa$  means the average of  $s^{-1}$  with respect to the Poisson distribution with parameter  $\kappa$ . In the limit

$\gamma \rightarrow 1$ , (24) becomes equivalent to the result of second-order Rayleigh–Schrödinger perturbation theory.

In the general case, the self-energy is a functional of the function  $\Omega_{\vec{K}'} = \omega - \xi_{\vec{K}'} = \omega - \eta - \Sigma_{\vec{K}'}^{(1)}$ , i.e., on the basis of (32), (33) we have

$$\Omega_{\vec{K}} = \text{Re}\Sigma_{\vec{K}}^{(2)}[\Omega_{\vec{K}'}] - \Sigma_{\vec{K}}^{(1)}, \quad (35)$$

and the dispersion relation becomes

$$E_{\vec{K}} = \Omega_{\vec{K}} - \varepsilon_p \gamma (2 - \gamma) + \Sigma_{\vec{K}}^{(1)}. \quad (36)$$

#### IV. POLARON BAND STRUCTURE

We are now in the position to discuss the single-particle band dispersion of the 2D Holstein model. In the first place, we can extract the  $\vec{K}$ -dependence of the so-called “coherent” energy band,  $E_{\vec{K}}$ , from the position of the lowest peak in each spectral function  $\mathcal{A}_{\vec{K}}$  using the ED data of Sec. 2.1 (cf. Fig. 2 d–f). This has been done in our previous work [19]. In the weak-coupling case and for phonon frequencies less than the bare electronic bandwidth, we have found a nearly unaffected tight-binding band near the band center and a practically flat region at larger momenta. As a result the coherent bandwidth  $\Delta E = \sup_{\vec{K}} E_{\vec{K}} - \inf_{\vec{K}} E_{\vec{K}}$  is roughly given by  $\omega_b$ .

The results for the intermediate-to-strong EP coupling regime are shown in Fig 5. Besides the well-known narrowing of the bandwidth ( $\Delta E/8t = 0.0814$ ), there are at least two features worth mentioning in the crossover region (see Fig. 5 a). Firstly, the exact band structure differs significantly from a simple tight-binding band having the same bandwidth. Moreover, because of further than NN hopping processes generated by the EP interaction, the enhancement of the effective mass is weakened near  $\vec{K} = 0$ . Secondly, it should be noted that the “flattening” of the band structure, discussed above for weak EP coupling, survives to relatively large EP interactions (even though  $\omega_b > 2\Delta E$ ). At this point we would like to stress that the finite-size effects are rather small, i.e. although the data points belong to different system sizes we found a remarkably smooth behaviour of  $E_{\vec{K}}$ .

In order to check for the applicability of the theory outlined in Sec. 3, we have compared  $E_{\vec{K}}$  given by (34) with the exact results, where the parameter  $\gamma$  was determined to reproduce the correct ground-state energy. As can be seen from Fig. 5 b, we found a surprisingly good agreement of the theoretical curve with the numerical data. It is natural to ask why our strong-coupling approach is so good even in the intermediate EP coupling situation. First of all, the second-order corrections to the self-energy involve longer-ranged polaron hopping processes due to (multi-) phonon absorption and emission. As mentioned above such processes are of particular importance in the crossover region. Thus we expect an even

better agreement including higher-order corrections [20]. The more important point, however, seems to be the use of the incomplete Lang–Firsov transformation in the derivation of (34). Obviously, both the Lang–Firsov formula ( $E_{\vec{K}} = -\varepsilon_p - 2t \exp\{-g^2\}(\cos K_x + \cos K_y)$ ) and standard second-order strong-coupling perturbation theory (SCPT) fail to describe the band dispersion correctly. Moreover, as might be expected, both approximation considerably overestimate the renormalization of coherent bandwidth for intermediate EP couplings and phonon frequencies. A discussion of the strong-coupling case will be given separately in the Appendix.

#### V. CONCLUSIONS

To summarize, in this paper we have performed a highly complete numerical analysis of the 2D Holstein model studying the effect of polaron formation. The emphasis was on the intermediate coupling regime, i.e., the transition region from nearly free electrons to small polarons. The calculations are carried out by exact diagonalization of finite systems including the full dynamics of phonons. Results are unbiased and allow to test a new theoretical approach applied to the calculation of the polaron self-energy as well as previously proposed theories. Our main results are the following:

- (i) In the 2D Holstein model a continuous transition from a nearly free electron to a small polaron takes place if both criteria,  $\lambda > 1$  and  $g^2 > 1$ , are satisfied, i.e.,  $\lambda$  and  $g^2$  are not by themselves independent parameters [19,15].
- (ii) The small polaron state is basically a multi-phonon state characterized by strong on-site electron-phonon correlations making the particle susceptible to self-trapping [13].
- (iii) Depending on the adiabatic ratio  $\alpha$ , there are two types of small polaron states in the very strong-coupling regime: the adiabatic Holstein polaron and the non-adiabatic Lang–Firsov polaron (cf. Appendix). By the use of the correct polaron theory, i.e. the adiabatic Holstein approximation and the canonical Lang–Firsov approach with appropriate corrections, one obtains an excellent estimate of the coherent bandwidth in both adiabatic and non-adiabatic regimes [11,34].
- (iv) The kinetic energy loss as a function of the EP coupling strength indicates that the “width” of the crossover region is rather small (broad) in the adiabatic (non-adiabatic) regime [21,15].
- (v) The single-particle spectral function shows the evolution of a well-separated narrow small polaron band with low spectral weight. On the other hand, composite particle operators, properly dressed by

dynamical phonons, give large spectral weight in the spectral function, i.e., they are much better fundamental excitations of the systems [16,25].

- (vi) At intermediate EP coupling strengths and phonon frequencies the effective polaronic band dispersion deviates substantially from a simple tight-binding cosine band due to further than nearest-neighbour ranged hopping processes generated by the EP interaction. The proposed theoretical strong-coupling approach, based on an incomplete Lang-Firsov transformation, yields a satisfactory description of the polaron band structure, whereas the standard Lang-Firsov and strong-coupling perturbation theories fail to give the correct energy dispersion (coherent bandwidth).
- (vi) The lineshape of the optical absorption spectra is highly asymmetric in the weak-to-intermediate coupling regime, whereby the optical response on the low-energy side of the absorption peak exceeds that on the high-energy side [26,12].

*Acknowledgements.* This work was supported in part by the Deutsche Forschungsgemeinschaft through SFB 279 B5, and by the Grant Agency of Czech Republic, Project No. 202/96/0864. Numerical calculations were carried out at the LRZ München, the HLRZ Jülich, and the HLR Stuttgart.

## APPENDIX

Here we would like to add some comments on the nature of the small polaron state in the strong-coupling limit of the Holstein model. There is some confusion in the literature, particularly about the use of the correct theory of polarons (with appropriate corrections, cf. Refs. [10–12]). This may be originated by the fact, that in the extreme strong-coupling limit both the adiabatic Holstein [2] and non-adiabatic Lang-Firsov [5] formulae, obtained from expansions in powers of  $\alpha \ll 1$  [2,35] and  $1/\lambda \ll 1$  [36], respectively, yield the same exponential band renormalization:  $\exp\{-g^2\}$ . However, the pre-exponential factors are different for any value of  $\lambda$  [12], and the generalized Holstein formula derived by Alexandrov and Mott [34] also contains essential corrections of the exponent,  $g^2 \rightarrow \bar{g}^2$ , at intermediate-to-strong EP couplings.

These findings are supported by exact diagonalizations, which we have performed for the 1D Holstein model at fixed  $g^2$  but different adiabatic ratios  $\alpha$ . The comparison of the exact results with the theoretical approaches is presented in Fig. 6. In the strong-coupling anti-adiabatic limit ( $g^2 = 5$ ,  $\alpha = 10$ ), where our theory coincides with the SCPT, we obtained an excellent agreement with the exact dispersion for all  $\vec{K}$ . Moreover, the simple

Lang-Firsov formula works perfectly well in the determination of the coherent bandwidth  $\Delta E_{LF} \simeq \Delta E = 0.027$ . This is in contrast to the adiabatic strong-coupling case ( $\alpha = 0.8$ ,  $\lambda = 2$ ,  $g^2 = 5$ ). Here the non-adiabatic Lang-Firsov and SCPT expressions are found to be quite inadequate, e.g., they underestimate the exact bandwidth  $\Delta E = 0.0562$  by more than a factor of two. Although the theory of Sec. 3 improves this result to some extent ( $\Delta E(\gamma = 0.97) = 0.0362$ ), a much better estimate of the bandwidth is achieved using the generalized Holstein formula [34]:  $\Delta E_{Ho} = 0.0577$ . In any case, in real solids the coherence of these small-polaron band states will be rapidly destroyed by thermal fluctuations and/or disorder effects.

- 
- [1] E. K. H. Salje, A. S. Alexandrov, and W. Y. Liang, *Polarons and Bipolarons in High Temperature Superconductors and Related Materials*, Cambridge Univ. Press, (Cambridge 1995).
  - [2] T. Holstein, Ann. Phys. **8**, 325 (1959); **8**, 343 (1959).
  - [3] D. Emin, Adv. Phys. **22**, 57 (1973).
  - [4] A. B. Migdal, Sov. Phys. JETP **7**, 999 (1958).
  - [5] I. G. Lang and Y. A. Firsov, Zh. Eksp. Teor. Fiz. **43**, 1843 (1962).
  - [6] F. Marsiglio, Physica C **244**, 21 (1995).
  - [7] I. B. Levinson and E. I. Rashba, Sov. Phys. Usp. **16** 892 (1974); E. I. Rashba, Synth. Met. **64**, 255 (1994).
  - [8] J. Zhong and H.-B. Schüttler, Phys. Rev. Lett. **69**, 1600 (1992).
  - [9] J. Ranninger and U. Thibblin, Phys. Rev. B **45**, 7730 (1992).
  - [10] F. Marsiglio, Phys. Lett. A **180**, 280 (1993).
  - [11] V. V. Kabanov and D. K. Ray, Phys. Lett. A **186**, 438 (1994).
  - [12] A. S. Alexandrov, V. V. Kabanov, and D. K. Ray, Phys. Rev. B **49**, 9915 (1994).
  - [13] G. Wellein, H. Röder, and H. Fehske, Phys. Rev. B **53**, 9666 (1996).
  - [14] G.-P. Borghi, A. Girlando, A. Painelli, and J. Voit, EuroPhys. Lett. **34**, 127 (1996).
  - [15] M. Capone, W. Stephan, and M. Grilli, Phys. Rev. B **56**, xxx (1997).
  - [16] J. M. Robin, cond-mat/9704237.
  - [17] E. V. L. de Mello and J. Ranninger, Phys. Rev. B **55**, 14872 (1997).
  - [18] W. Stephan, Phys. Rev. B **54**, 8981 (1996).
  - [19] G. Wellein and H. Fehske, Phys. Rev. B **56**, xxx (1997).
  - [20] G. Polatsek and K. W. Becker, preprint (1997).
  - [21] H. Fehske, H. Röder, G. Wellein, and A. Mistriotis, Phys. Rev. B **51**, 16582 (1995).
  - [22] Y. Inada and C. Ishii, J. Phys. Soc. Jpn. **59**, 612 (1990).
  - [23] R. N. Silver et al., J. of Comp. Phys. **124**, 115 (1996).
  - [24] E. Dagotto, Rev. Mod. Phys. **66**, 763 (1994).
  - [25] T. Sakai, D. Poilblanc, and D. J. Scalapino, Phys. Rev. B **55**, 8445 (1997).

- [26] D. Emin, Phys. Rev. B **48**, 13691 (1993).
- [27] G. D. Mahan, *Many-Particle Physics*, Plenum Press, (New York, London 1990).
- [28] A. S. Alexandrov, V. V. Kabanov, and D. K. Ray, Physica C **224**, 247 (1994).
- [29] J. Schnakenberg, Z. Phys. **190**, 209 (1966).
- [30] H. Fehske et al., Z. Phys. **94**, 91 (1994).
- [31] J. Loos, Z. Phys. B **96**, 149 (1994).
- [32] L. P. Kadanoff and G. Baym, *Quantum Statistical Mechanics*, Benjamin/Cumming Publishing Company, (Reading, Massachusetts 1962).
- [33] J. Loos, Phys. Status Solidi B **128**, 797 (1985).
- [34] A. S. Alexandrov and N. F. Mott, Rep. Prog. Phys. **57**, 1197 (1994).
- [35] E. I. Rashba, in *Excitons*, edited by E. I. Rashba and D. M. Struge, Nauka, (Moscow 1985).
- [36] A. A. Gogolin, Phys. Status Solidi **109**, 95 (1982).

FIG. 1. Phase diagram of the 2D Holstein model obtained for a 256-site square lattice using the variational Lanczos approach proposed by the authors in Ref. [21]. This technique, based on an inhomogeneous variational Lang-Firsov transformation, correctly reproduces the adiabatic ( $\alpha \ll 1$ ) and anti-adiabatic ( $\alpha \gg 1$ ), weak- ( $\lambda \ll 1$ ) and strong-coupling ( $\lambda, g^2 \gg 1$ ) limits. We stress that there is no true phase transition between the nearly free electron and small polaron states, i.e., the transition line only indicates the crossover region.

FIG. 2. Single-particle spectral function  $\mathcal{A}_{\vec{K}}(E)$  (thin lines) and partial integrated density of states  $\mathcal{N}_{\vec{K}}(E)$  (bold lines) for the 2D Holstein model with 18 sites at  $\lambda = 0.125$ ,  $\alpha = 0.8$  (left column, **a-c**) and  $\lambda = 1.25$ ,  $\alpha = 1.5$  (right column, **d-f**). The  $\vec{K}$ -values are given in units of  $\pi/3$ . Here and in the following all energies are measured in units of  $t$ .

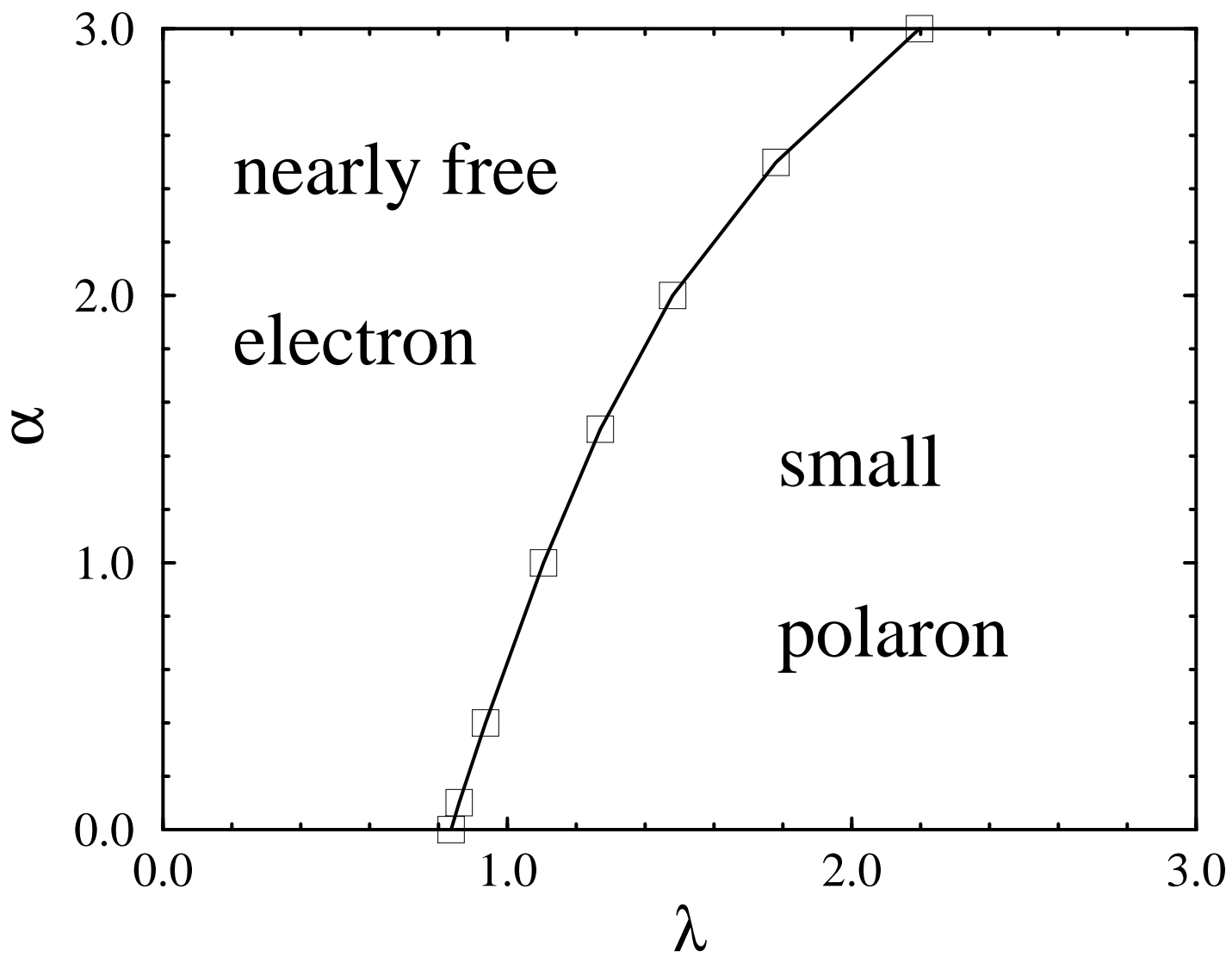
FIG. 3. Weight of the  $m$ -phonon states  $|c^m|^2$  (**a**) and wave-function renormalization  $\mathcal{Z}^{(c)}$  [ $\mathcal{Z}^{(d)}$ ] of a single electron (**b**) in the  $\vec{K} = 0$  ground state of the 2D Holstein model with ten sites. The residue of the “quasiparticle” pole shown in **b** was calculated using both the bare (open symbols) and dressed electron (filled symbols) operators. For further explanation see text.

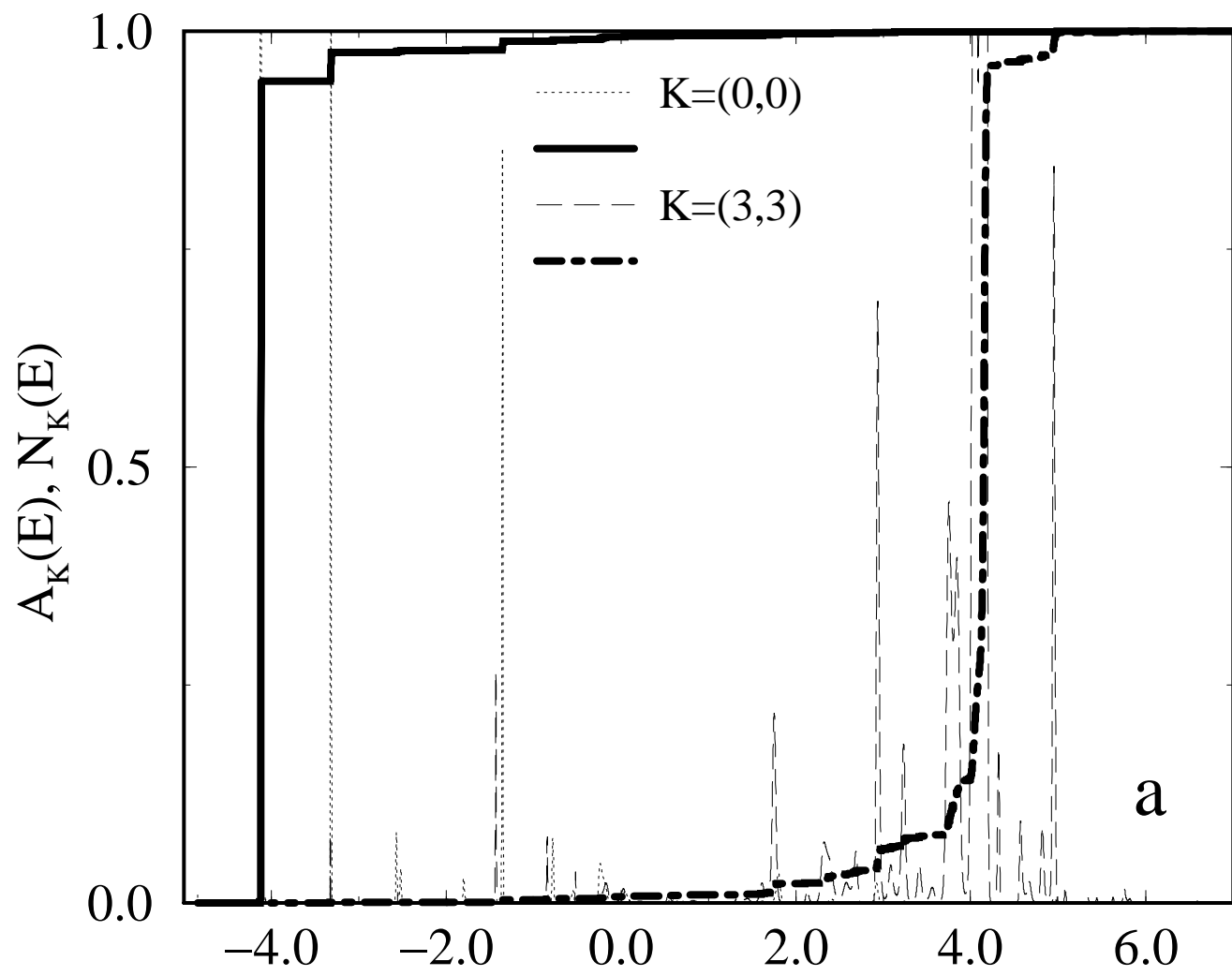
FIG. 4. Optical absorption in the 2D Holstein model. Using PBC, results for the regular part of the conductivity,  $\sigma_{xx}^{reg}$  and  $\mathcal{S}^{reg}(\omega)$ , are obtained for the 18-site lattice with  $M = 10$  phonons (**a**), whereas the various contributions to the sum rule are calculated on a ten-site lattice with  $M = 16$  phonons (**b**).

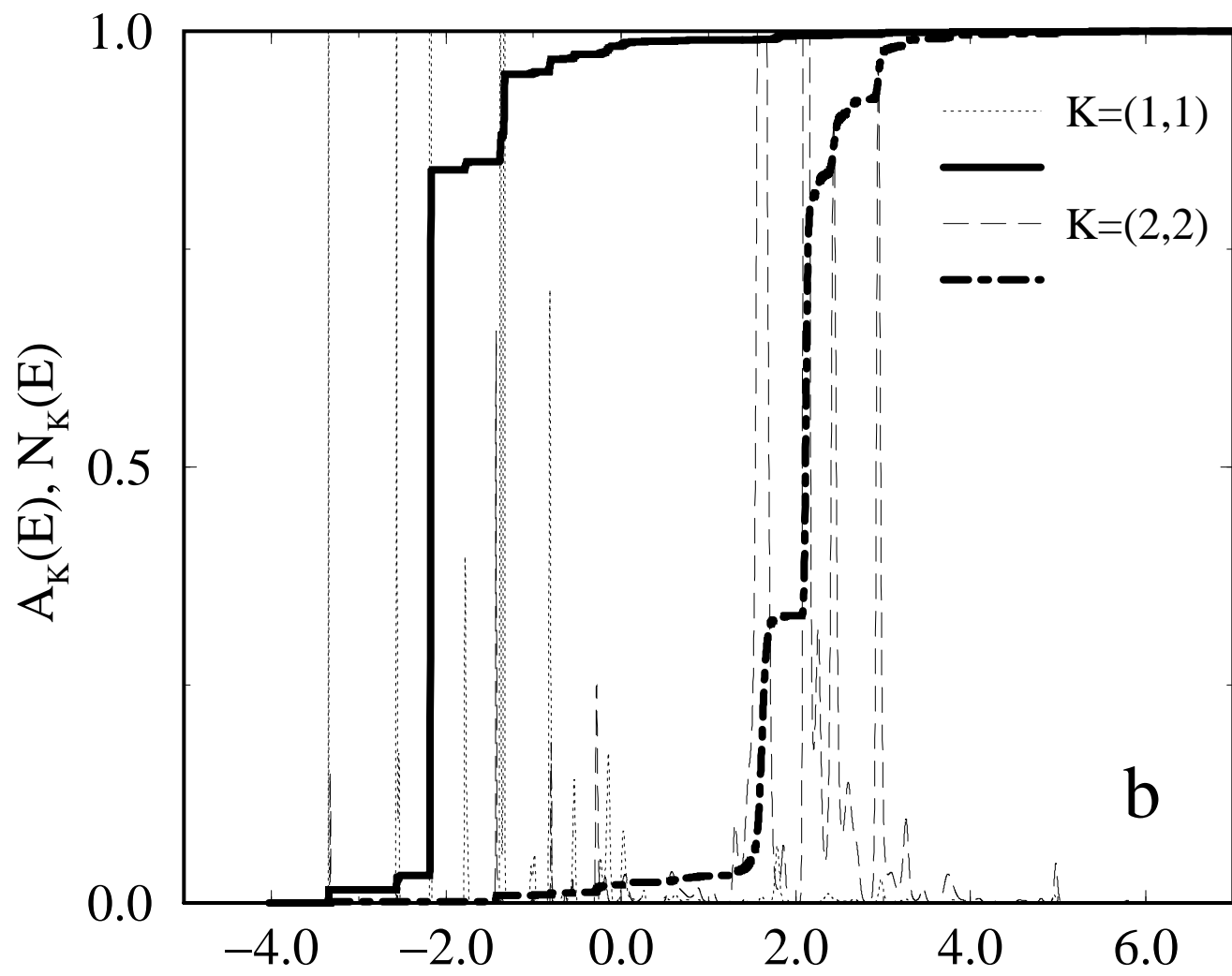
FIG. 5. Band dispersion of the 2D Holstein model along the highly symmetric directions of the Brillouin zone. In **a**, the exact results obtained for finite lattices with  $N = 16$  and 18 sites are compared with a rescaled tight-binding band (dotted line). The solid line is a least-squares fit to the ED data. In **b**, the chain-dashed line gives the band structure according to the theory developed in Sec. 3. Long- and short-dashed lines are the results of the Lang-Firsov approximation and the second-order SCPT, respectively.

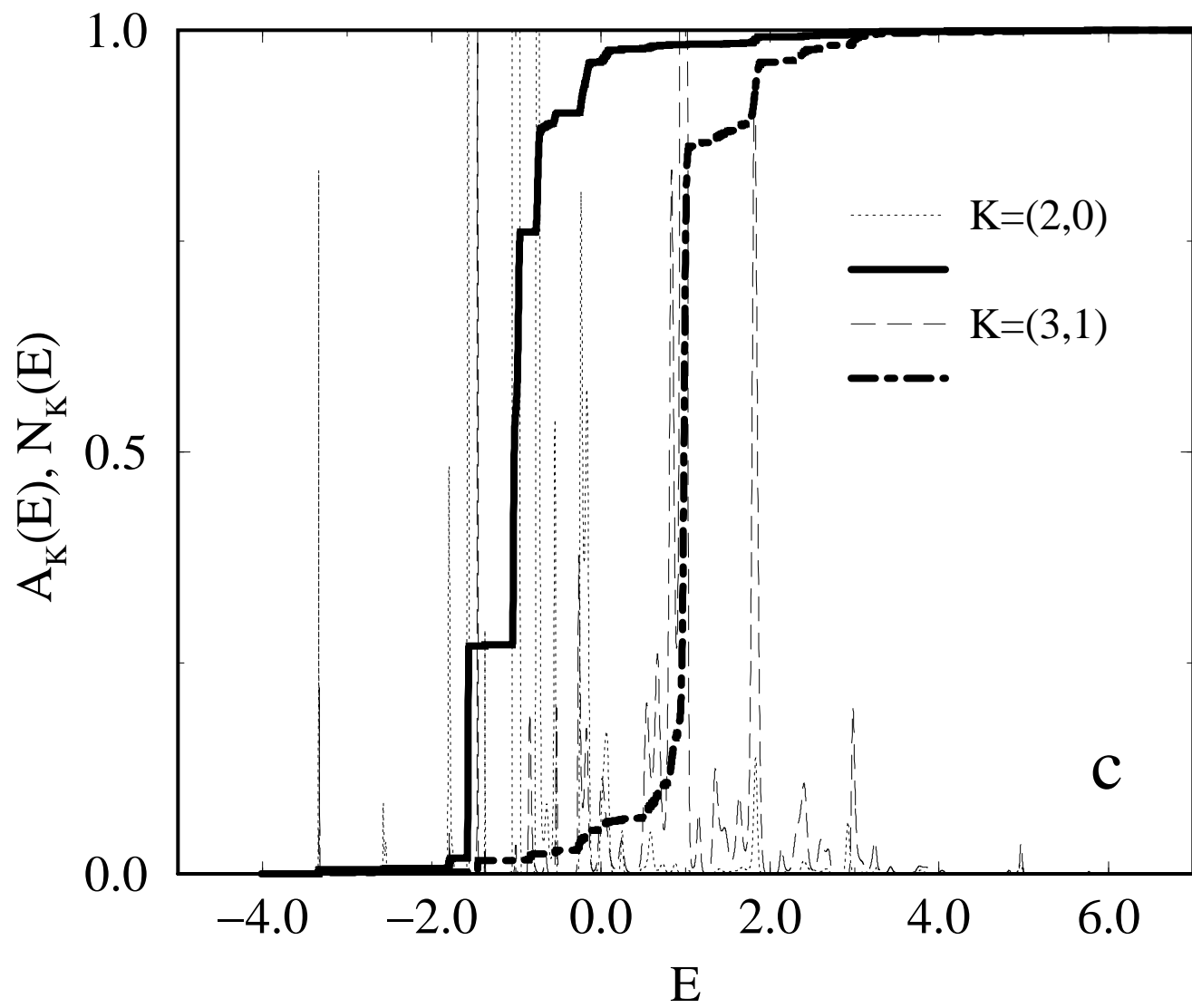
FIG. 6. Small polaron band dispersion for the 1D Holstein model. Exact results are compared with the predictions of different analytical approaches in the adiabatic ( $\alpha = 0.8$ ) and anti-adiabatic ( $\alpha = 10$ ) strong-coupling cases ( $g^2 = 5$ ,  $\lambda > 1$ ).

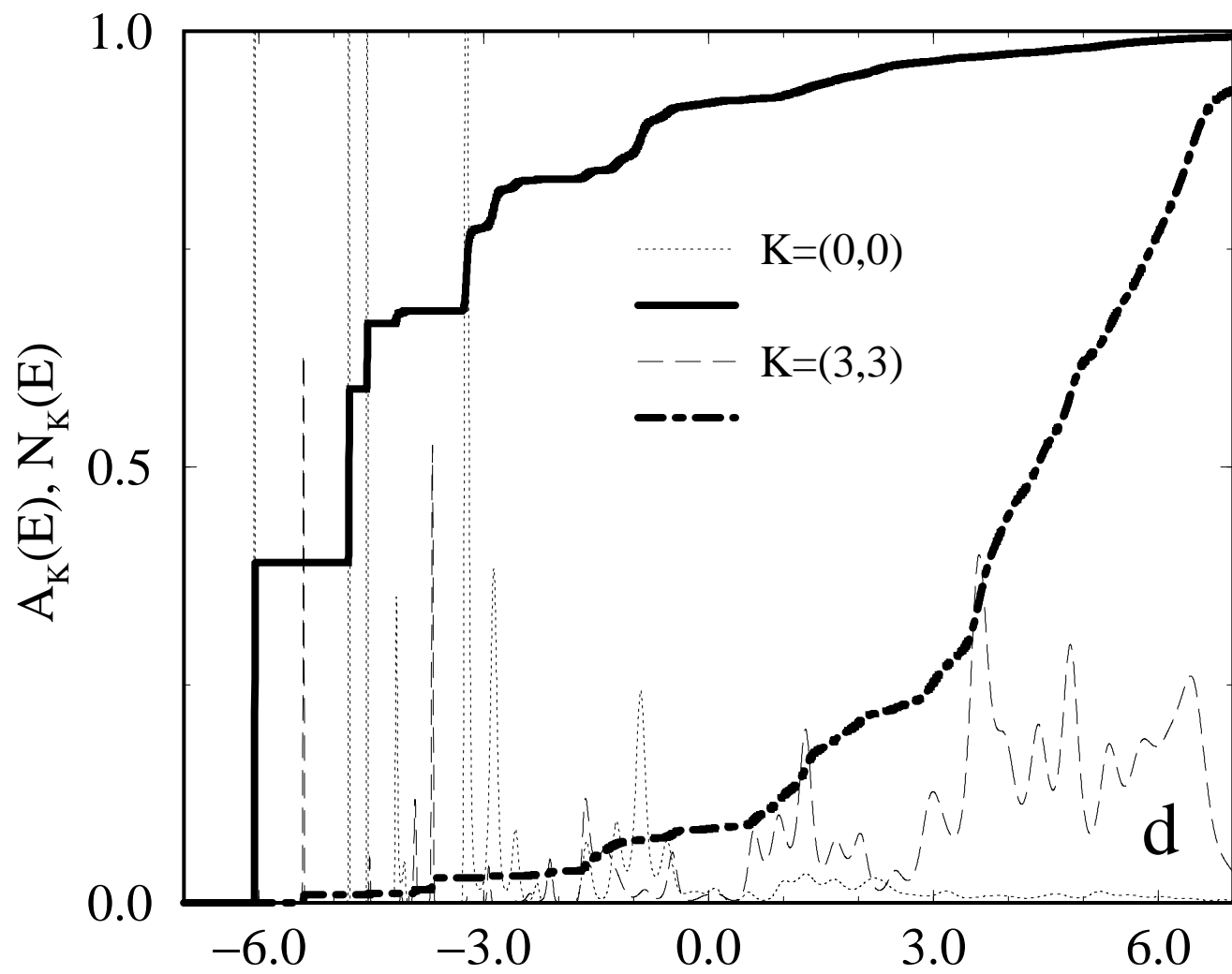


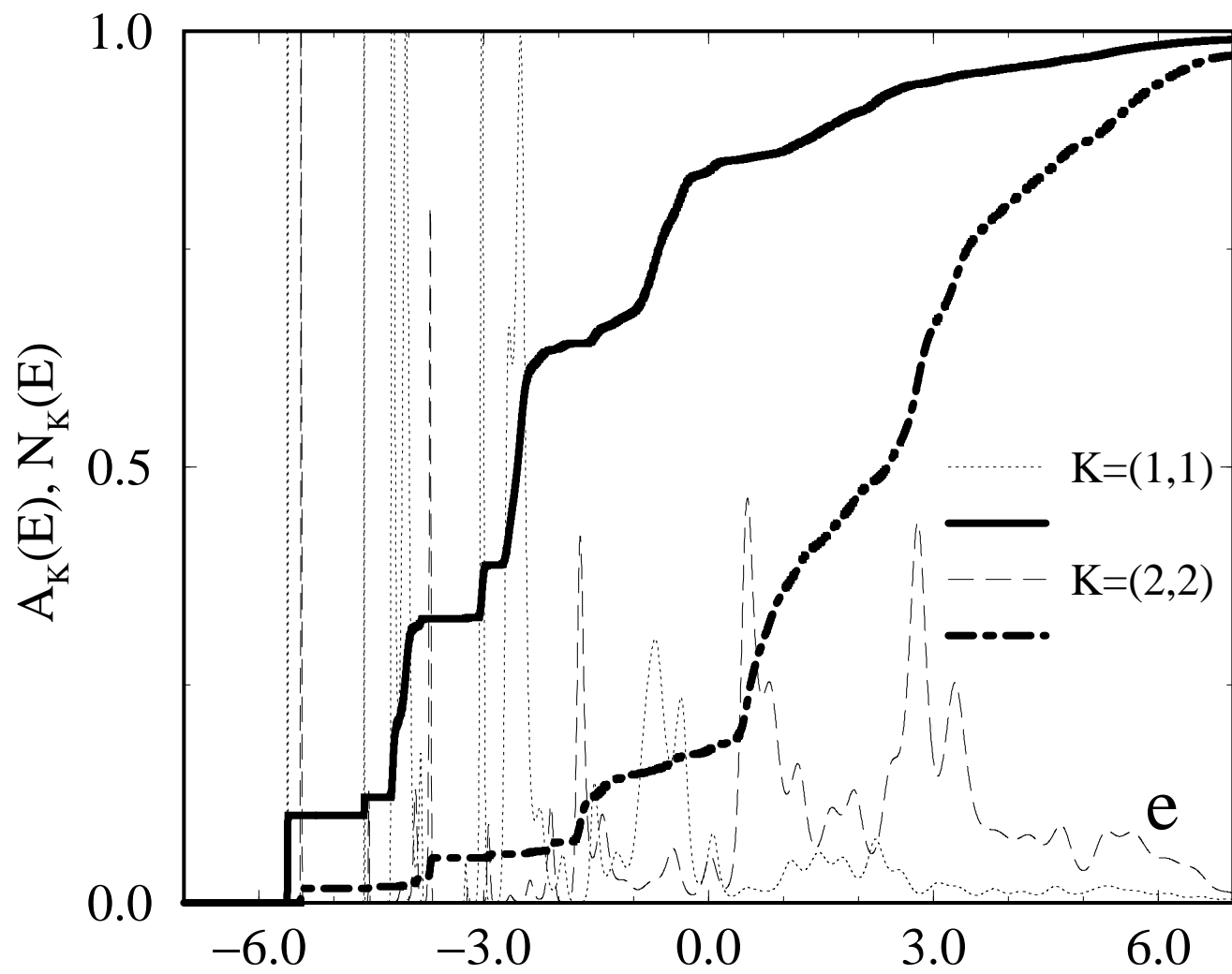


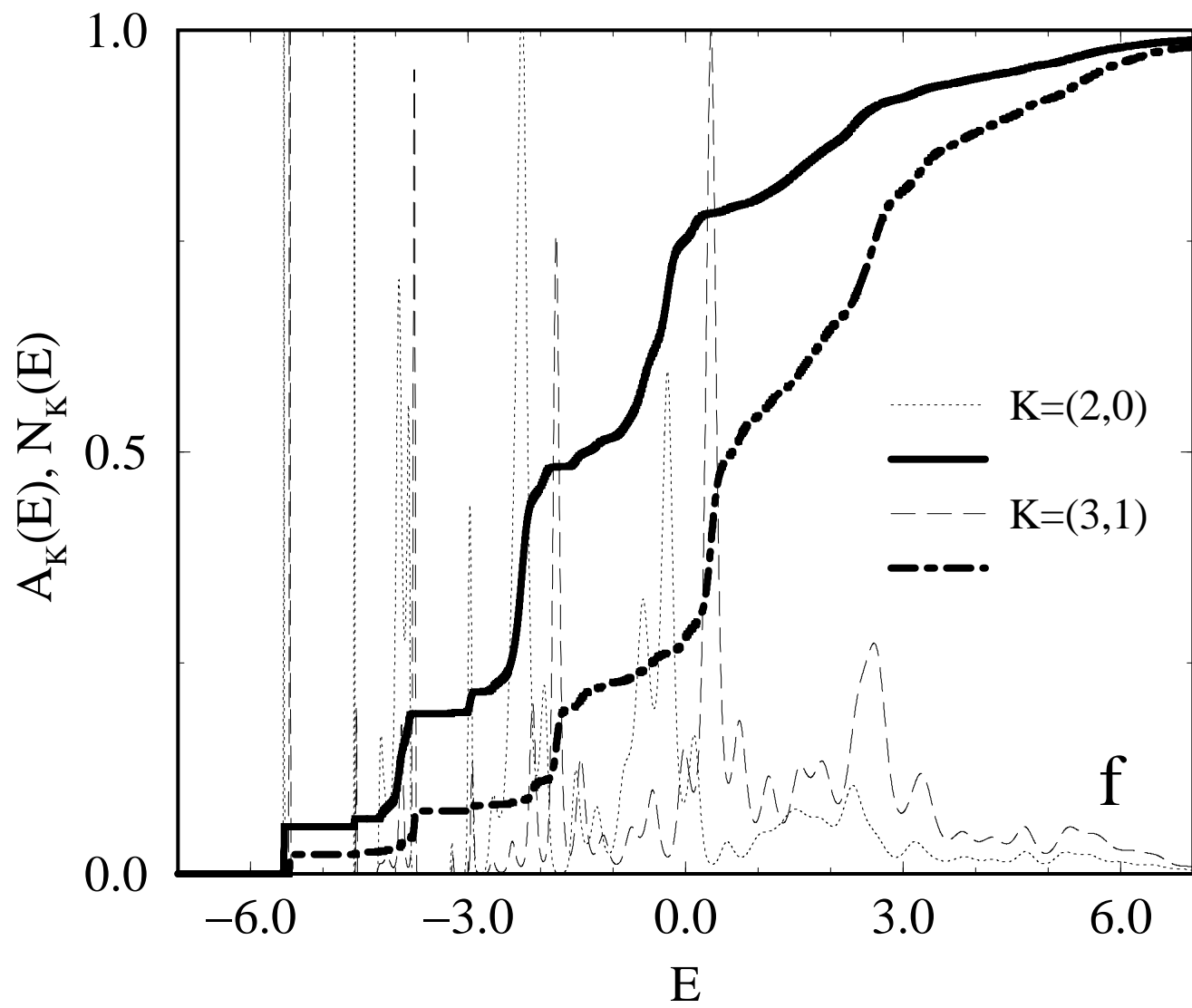


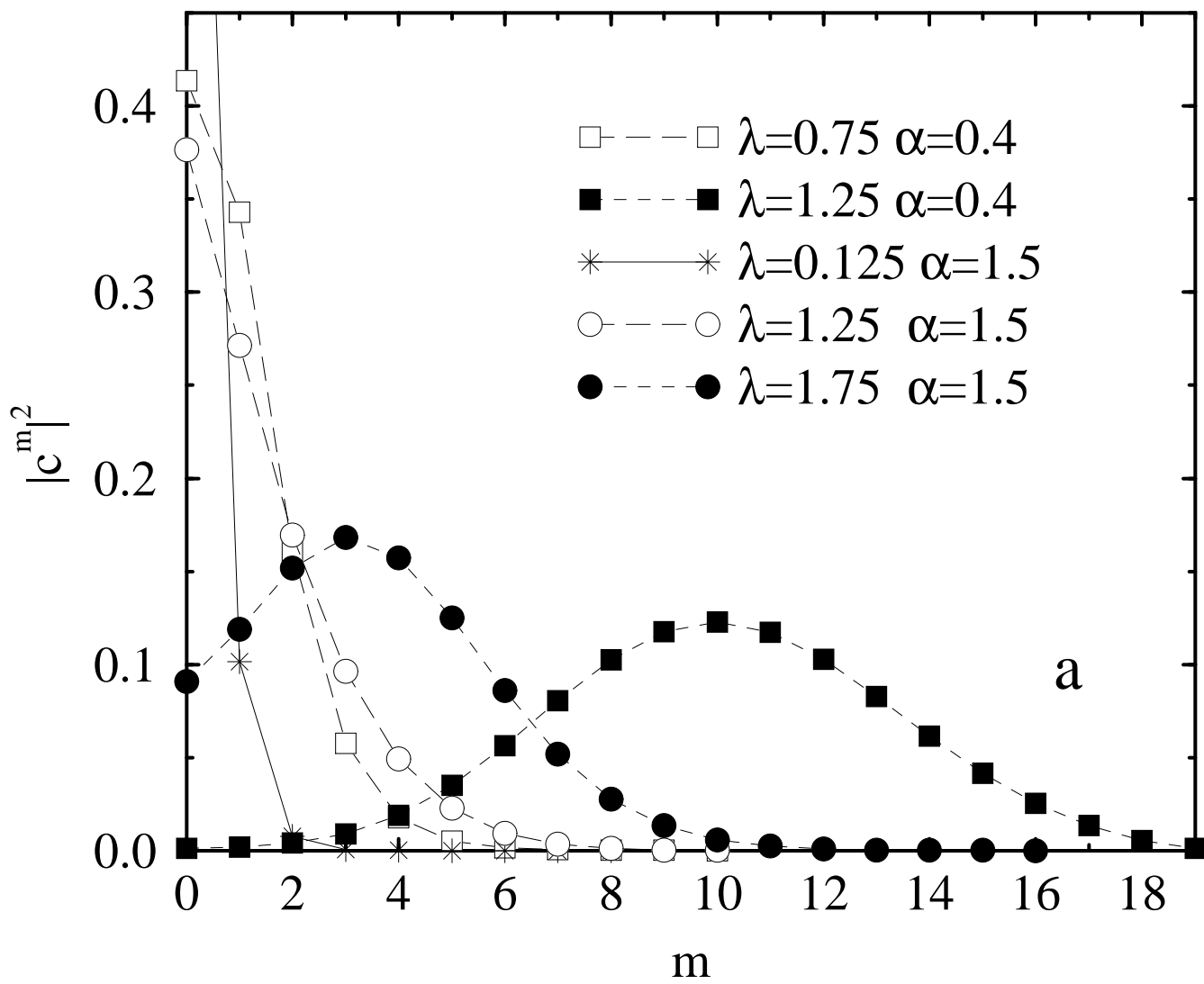




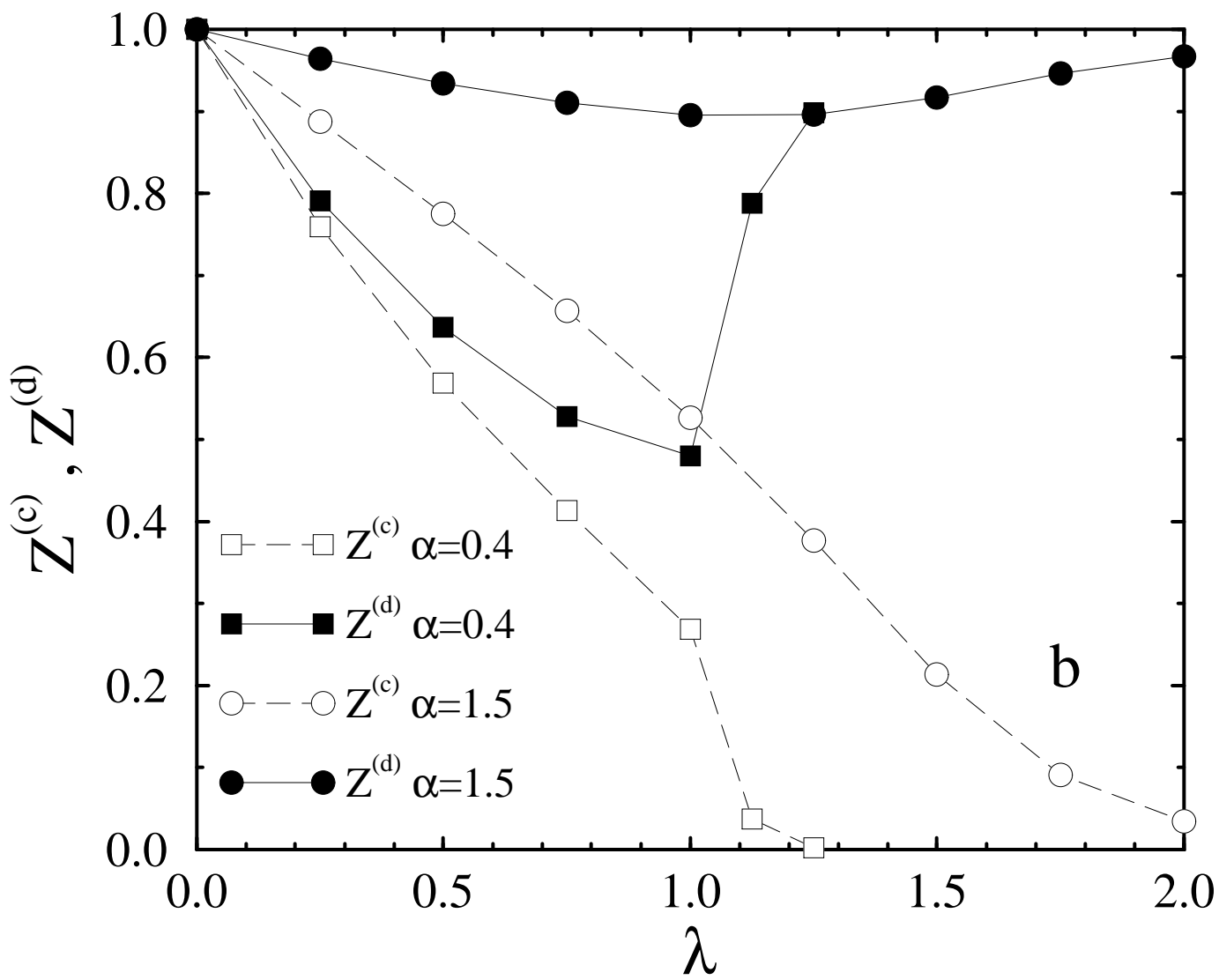


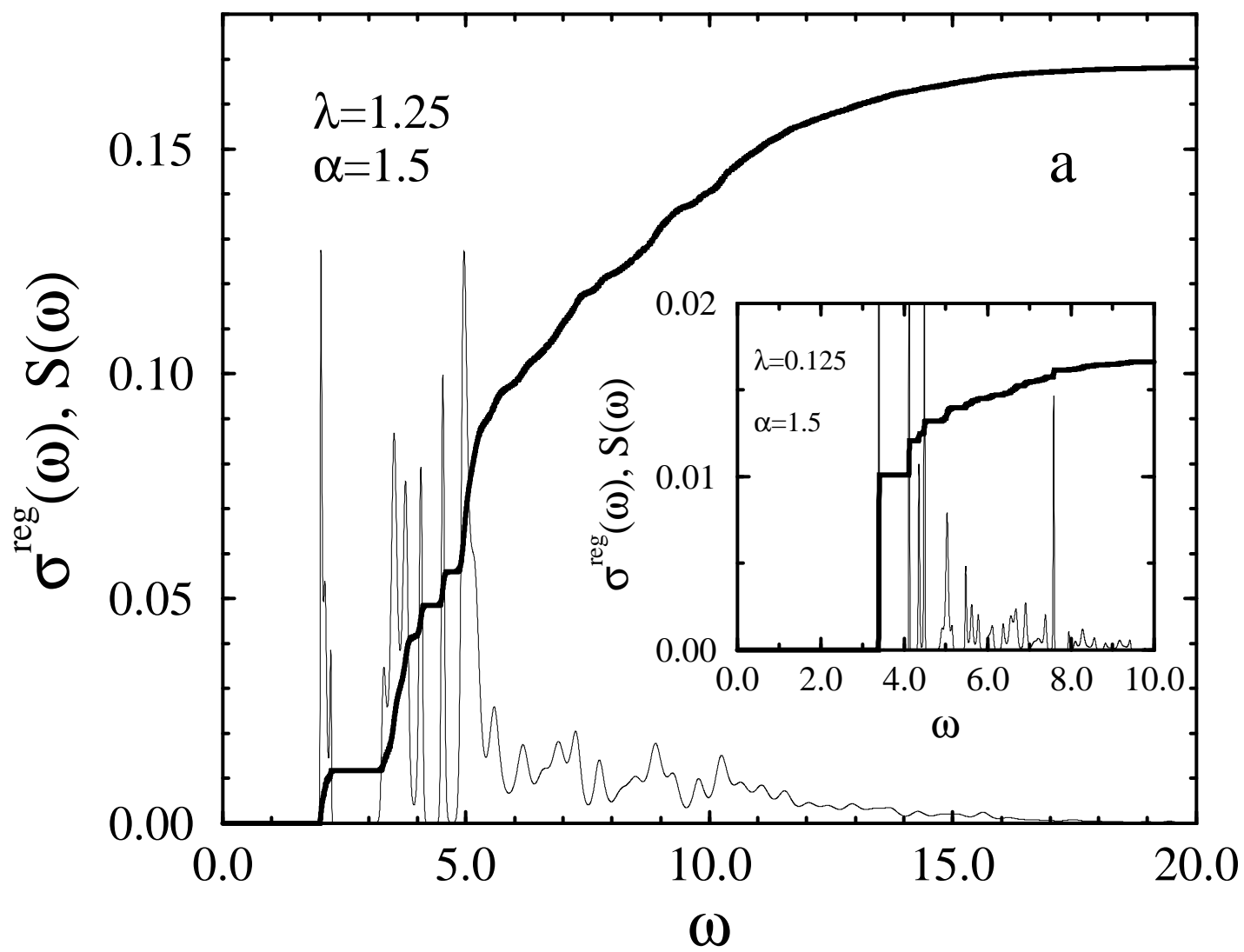


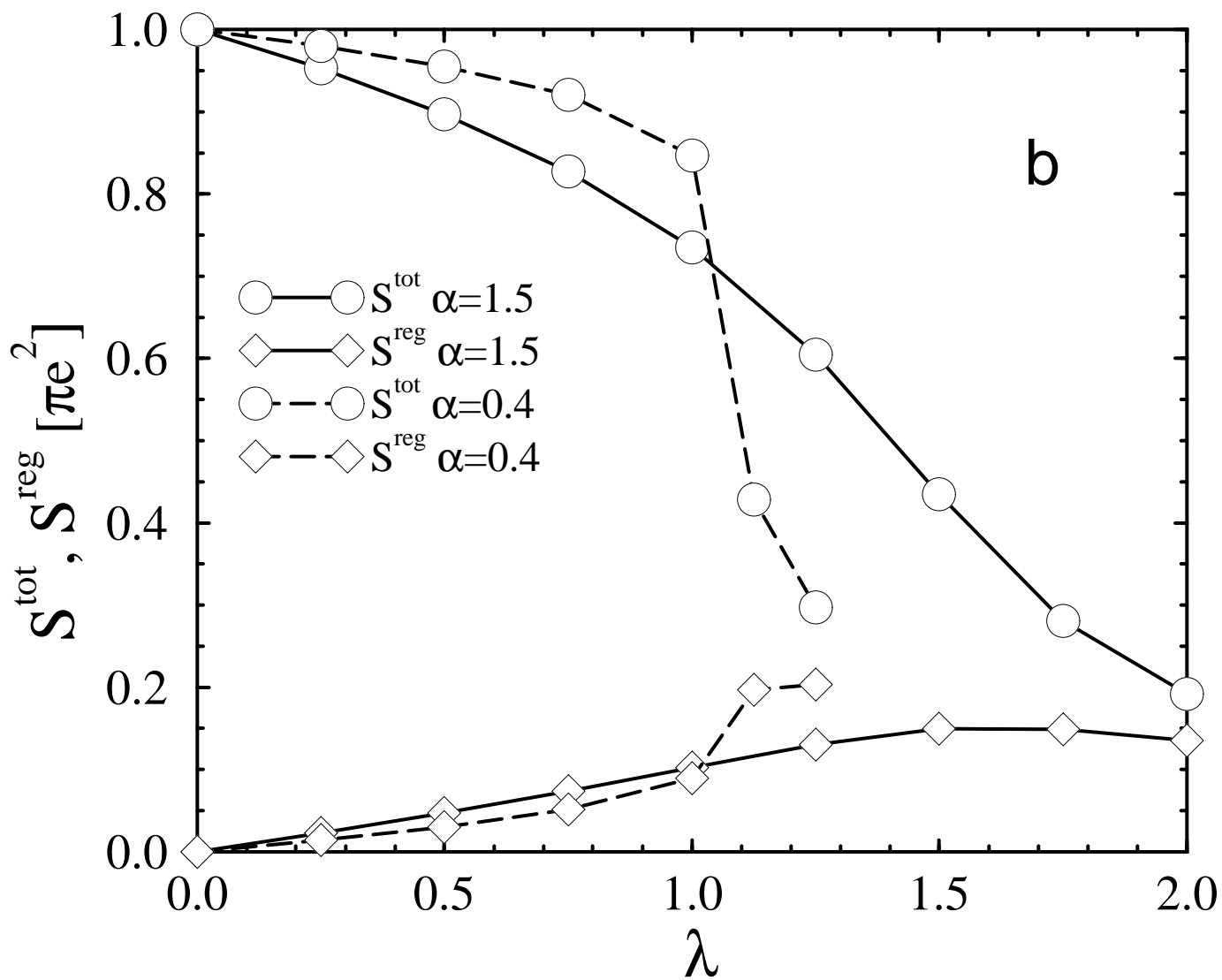


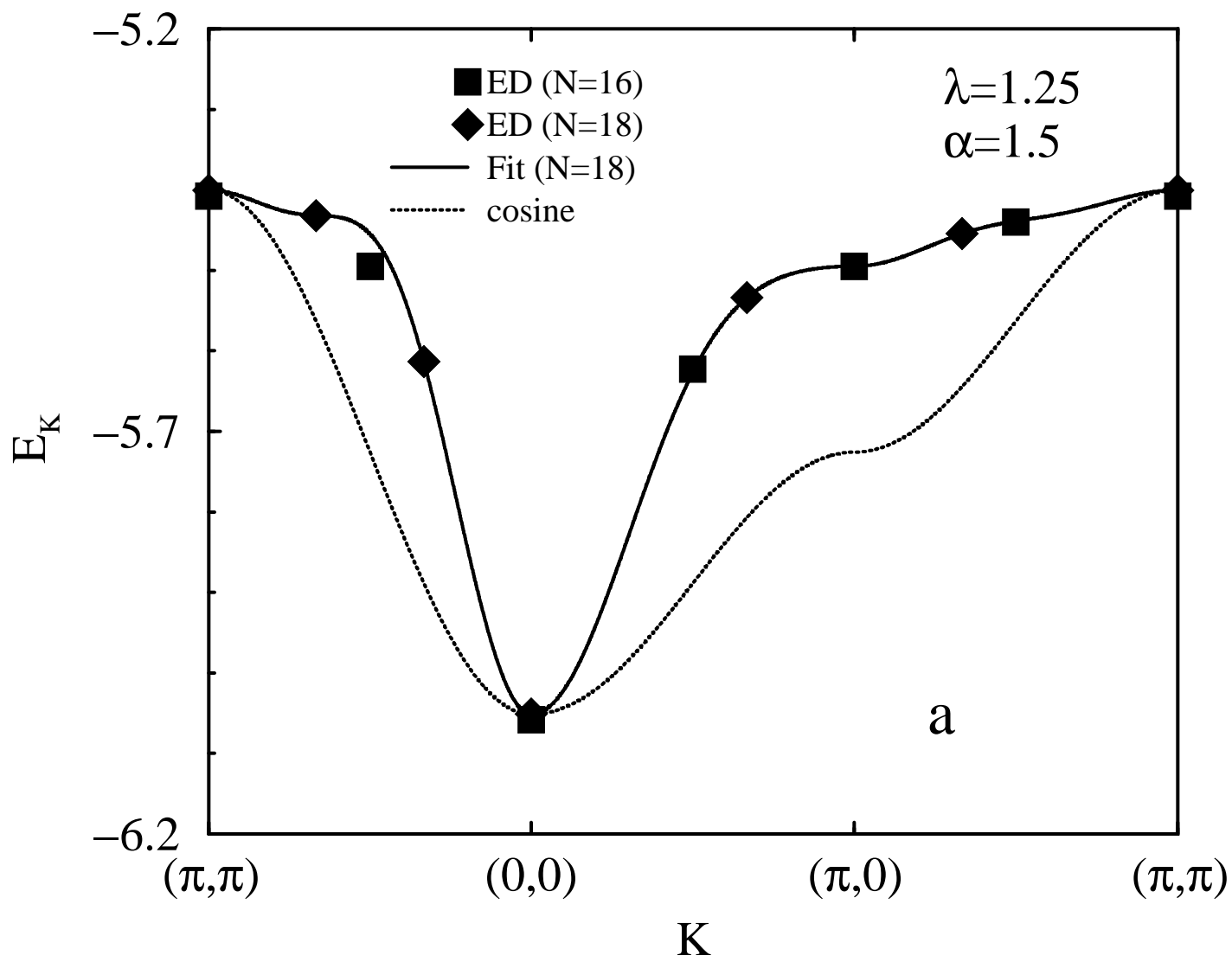


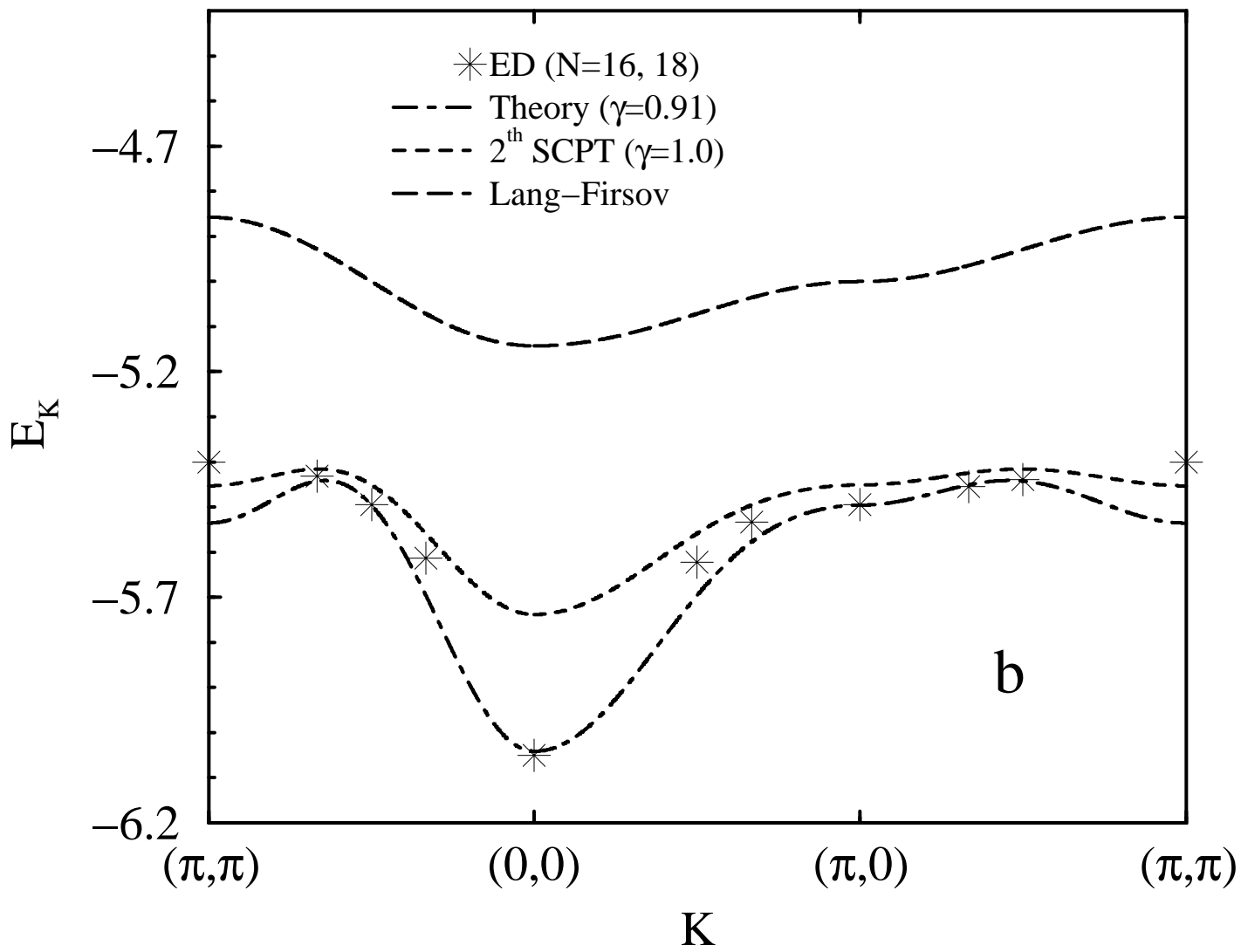












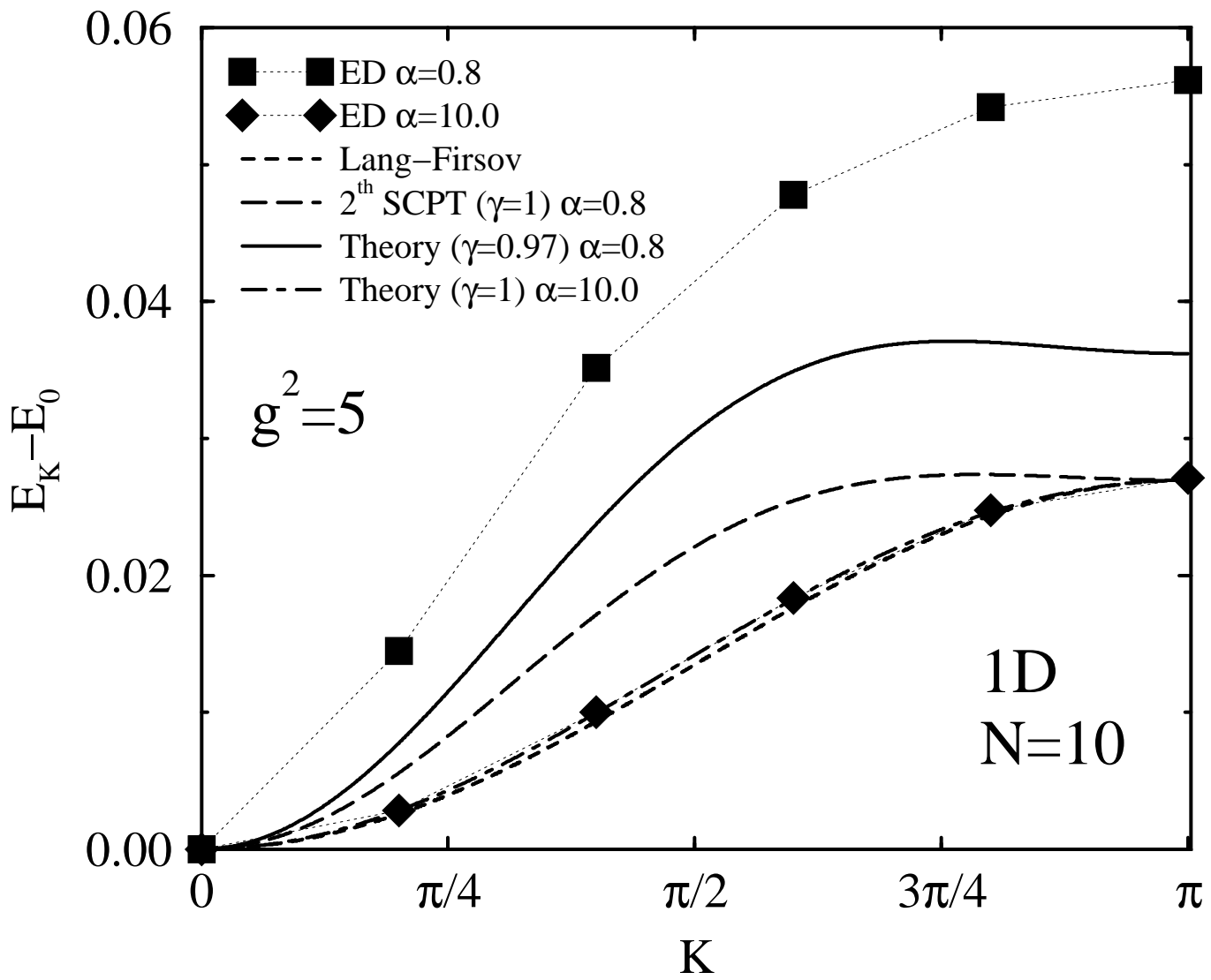


Figure 1:

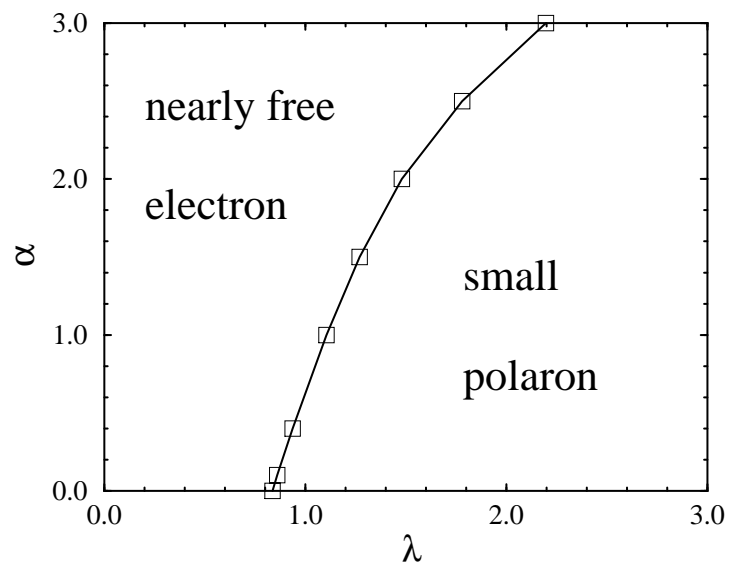


Figure 2:

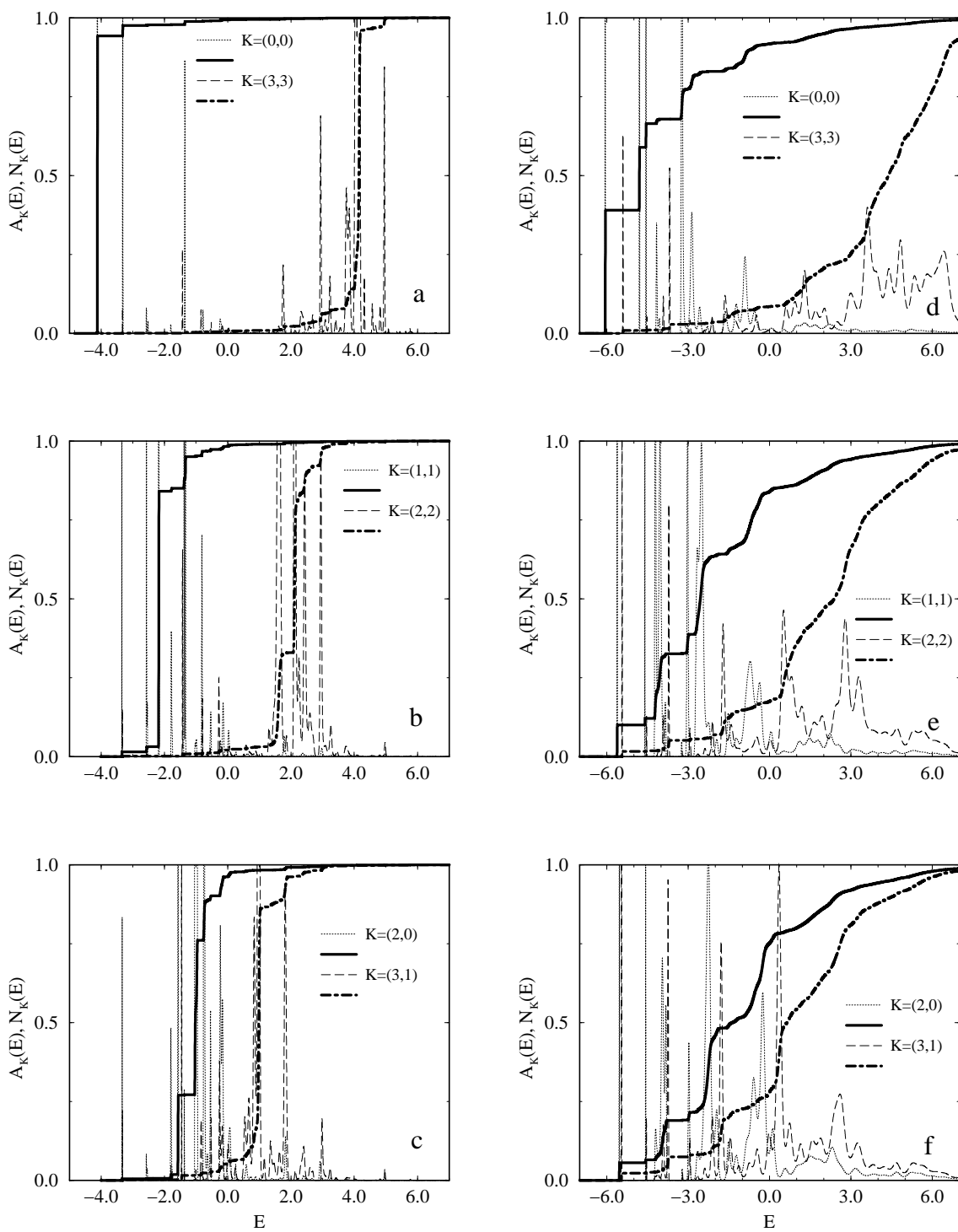




Figure 3:

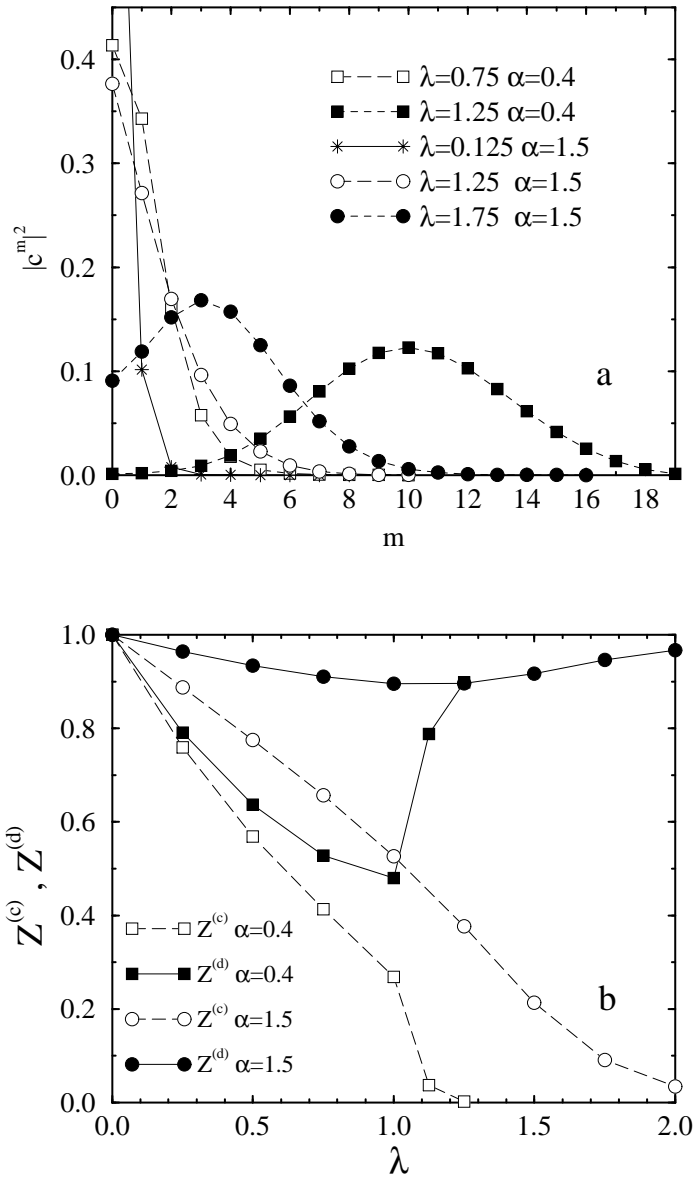


Figure 4:

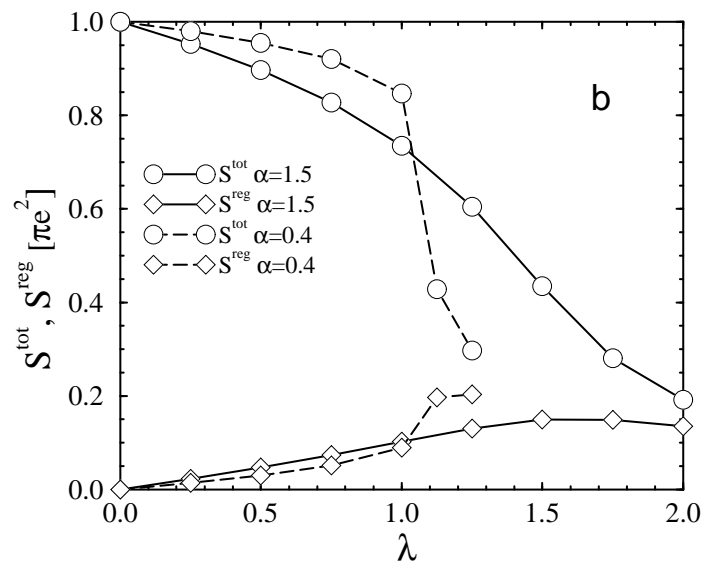
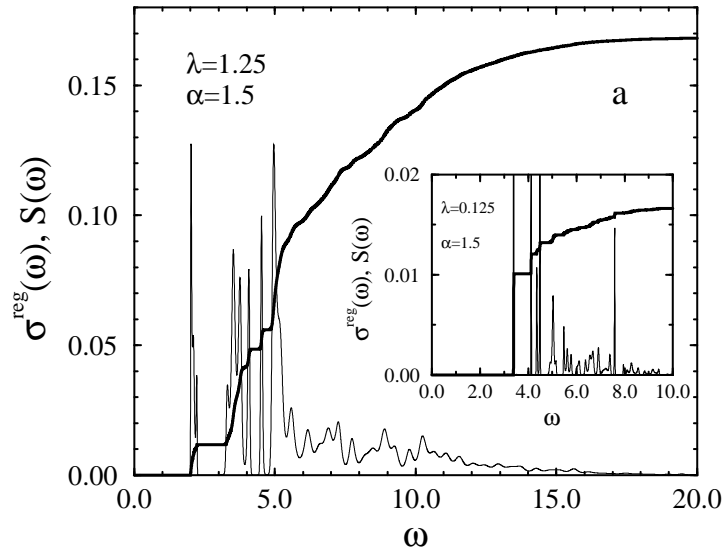


Figure 5:

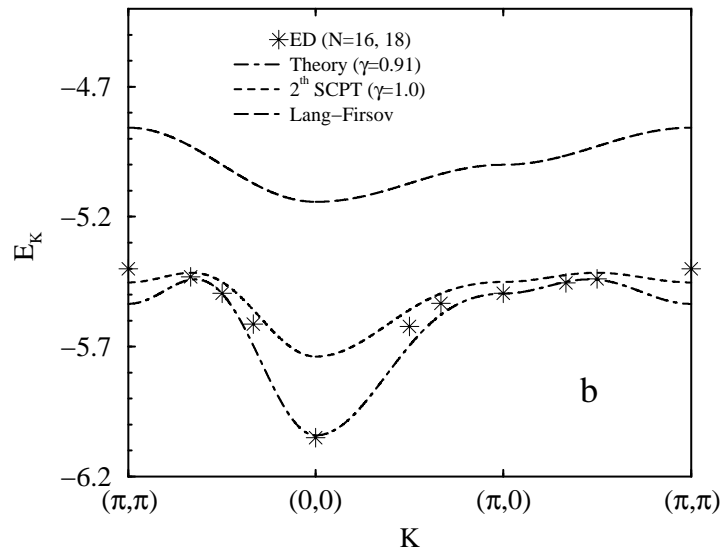
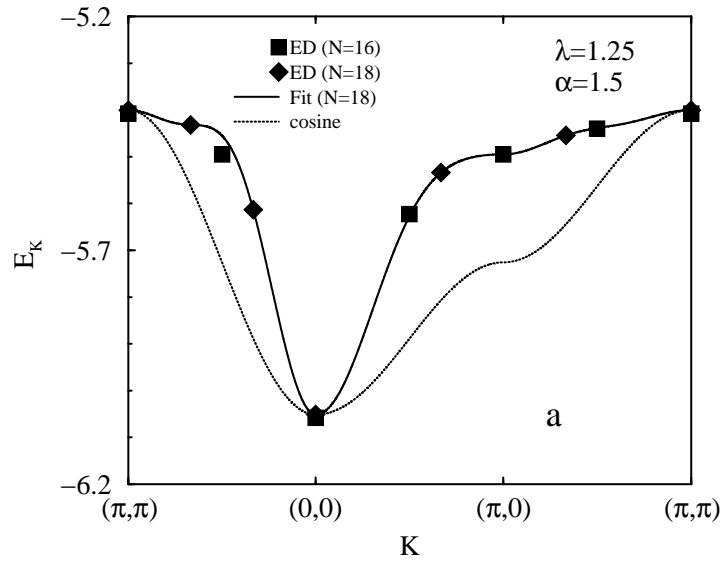


Figure 6:

